Calibration of an IMU-Camera Cluster Using Planar Mirror Reflection and Its Observability Analysis

Ghazaleh Panahandeh, *Student Member, IEEE,* Magnus Jansson, *Member, IEEE,*
and Peter Händel, *Senior Member, IEEE*

***Abstract*—This paper describes a novel and a low-cost calibration approach to estimate the relative transformation between an inertial measurement unit (IMU) and a camera, which are rigidly mounted together. The calibration is performed by fusing the measurements from the IMU-camera rig moving in front of a planar mirror. To construct the visual observations, we select a set of key features attached to the visual inertial rig where the 3D positions of the key features are unknown. During calibration, the system is navigating in front of the planar mirror while the vision sensor observes the reflections of the key features in the mirror, and the inertial sensor measures the system's linear accelerations and rotational velocities over time. Our first contribution in this paper is studying the observability properties of IMU-camera calibration parameters. For this visual inertial calibration problem, we derive its time-varying nonlinear state-space model and study its observability properties using the Lie derivative rank condition test. We show that the calibration parameters and the 3D position of the key features are observable. As our second contribution, we propose an approach for estimating the calibration parameters along with the 3D position of the key features and the dynamics of the analyzed system. The estimation problem is then solved in the unscented Kalman filter framework. We illustrate the findings of our theoretical analysis using both simulations and experiments. The achieved performance indicates that our proposed method can conveniently be used in consumer products like visual inertial based applications in smartphones for localization, 3D reconstruction, and surveillance applications.**

Fig. 1: An illustration of a potential application of the mirror-based IMU-camera calibration procedure for a smartphone, which has an embedded IMU and a camera. The figure shows a smartphone (to the right) and its mirror image (to the left). The logo of the phone (pear) can be considered as an object whose features' reflections in the mirror are in the camera's field of view.

I. Introduction

Recent improvements in inertial navigation systems allow for the building of small, lightweight, and cheap motion capture systems. Visual inertial navigation systems are natural extensions of inertial navigation systems, which are common in a variety of instrumentation and measurement applications like vehicle and autonomous applications [1], behavioral analysis [2], and biomedical applications [3]. Of particular interest is the fusion of an inertial measurement unit (IMU), as an inertial sensor, with a monocular camera, as a visual sensor, [4]–[6]. However, accurate information fusion between the sensors requires sensor-to-sensor calibration [7]–[11]. That is, estimating the 6-DoF transformation (the relative rotations and translations) between visual and inertial coordinate frames; disregarding such a transformation will introduce un-modeled biases in the system that may grow over time.

The problem of visual inertial calibration has been extensively investigated during the last decade [12]–[18]. For instance in [12], the estimation of relative rotation is performed using a calibration target that is vertically aligned with the direction of gravity. Then the relative translation is estimated using a turntable. In [14], the calibration is done via tracking of feature points on a calibration target, where the positions of the features are known. Alternative solutions are proposed in [16], both with and without using a calibration target with known landmarks, to estimate the 6-DoF transformation between the sensors.

In this paper, we propose a practical visual inertial calibration method, which is based on visual observations taken in front of a planar mirror, see Fig. 1. With the smartphone becoming a ubiquitous personal device, the need for simple yet effective calibration schemas has increased. Using a mirror as studied in our work is a pragmatic yet effective way to handle the calibration. In our proposed calibration method, the visual inertial system is navigating in front of the planar mirror, while the camera observes a set of features' reflections (known as *key features*) in the mirror. The key features are considered to be static with respect to the camera, and such that their reflections can always be tracked over images. For this nonlinear system, we derive the state-space model, and estimate the calibration parameters along with other system state variables using the unscented Kalman filter [19]. A primary study of the estimation problem was given in [17], where the results were only evaluated using simulation data. In our previous work [20], the problem of estimating camera intrinsic parameters together with IMU-camera calibration parameters has been studied in a similar framework; however, compared to the proposed method in this paper and [17], the

The authors are with Department of Signal Processing, ACCESS Linnaeus Centre, KTH Royal Institute of Technology, SE-10044 Stockholm, Sweden. email: {ghpa, janssonm, ph}@kth.se

positions of the key features were assumed to be a priori known and the evaluation was performed only with simulation data.

Unlike the current calibration approaches in [12], [14], [15], [21], our method does not rely on a direct view of a static calibration pattern with known feature point positions. Arbitrary feature points are selected in the camera body where no prior knowledge is assumed on the pose of the feature points relative to the camera's optical center. Moreover, contrary to the existing approach in [22], [23], no restriction in the IMU-camera movement is considered except the existence of the virtual features in the recorded images.

The main contributions of this paper are summarized as follows: First, we perform the observability analysis of the proposed IMU-camera time-varying nonlinear system. To the best of our knowledge, we are the first to perform such an analysis for the mirror-based visual inertial calibration. The analysis, although cumbersome, is important to guarantee the feasibility of the proposed calibration procedure. Accordingly, a major part of the results are reported in the appendices of the paper. We perform the observability analysis for this complex model using only two key features, and prove that the calibration parameters, as well as the 3D positions of the key features with respect to the camera, are observable. This means that given sufficient measurements from the visual and inertial sensors, we can estimate the unknown constant parameters along with the dynamics of the system. Secondly, for the analysed IMU-camera sensor fusion system, we derive the nonlinear state-space formulation and estimate the calibration parameters, 3D position of key features, and the dynamics of the system using the unscented Kalman filter. Finally, the theoretical findings of our observability analysis and estimation approach are validated both with simulations and experiments. We believe that the simplicity, flexibility, and low computational cost make our proposed scheme suitable for many different applications. The system can be conveniently used in, e.g., smartphones, and without having access to a calibration target.

The paper is organized as follows: Notations are given in Section II. The general system descriptions, including experimental setup, the process and the measurement models are presented in Section III. Then, for the proposed system, the nonlinear observability analysis is performed in Section IV. The estimation framework is described in Section V. Performance evaluation is given in Section VI. Finally, the conclusion is presented in Section VII.

II. Notation

In the following sections, scalars are denoted by lowercase letters (s), vectors by bold letters ($\mathbf{f}$), and matrices by bold capitals ($\mathbf{K}$). $\mathbf{I}_m$ denotes the $m \times m$ square identity matrix and $\mathbf{0}_{m\times n}$ represents the $m \times n$ zero matrix. $\mathbf{e}_i \in \mathbb{R}^3$ for $i \in \{0,1,2,3\}$ are defined as: $\mathbf{e}_0 = [0\ 0\ 0]^\top$, $\mathbf{e}_1 = [1\ 0\ 0]^\top$, $\mathbf{e}_2 = [0\ 1\ 0]^\top$, and $\mathbf{e}_3^\top = [0\ 0\ 1]^\top$, where the superscript $\top$ denotes matrix transpose.

${}^A\mathbf{p}_B$ represents the position of coordinate frame $\{B\}$ in coordinate frame $\{A\}$, and ${}^A\mathbf{v}_B$ denotes the velocity of coordinate frame $\{B\}$ in coordinate frame $\{A\}$. Moreover, the 3D position of a key feature and its corresponding reflection in the mirror with respect to the camera frame are represented by ${}^C\mathbf{p}_f$ and ${}^C\acute{\mathbf{p}}_f$, respectively.

Based on the Euler rotation theorem, the principle rotation vector θ is defined as $\theta = \alpha\hat{\mathbf{k}}$ [24], where $\hat{\mathbf{k}}$ is the unit vector along the axis and α the angle of rotation. To represent the attitude, we use both the quaternion, $\mathbf{q} \in \mathbb{R}^{4\times 1}$, and the Cayley-Gibbs-Rodrigues parameterization, $\mathbf{s} \in \mathbb{R}^{3\times 1}$; where $\mathbf{s} = \tan(\frac{\alpha}{2})\hat{\mathbf{k}}$. Then, ${}^A\mathbf{q}_B$ and ${}^A\mathbf{s}_B$ are used to denote the orientation of the frame $\{B\}$ in the frame of reference $\{A\}$; $\mathbf{C}(\mathbf{q})$ and $\mathbf{C}(\mathbf{s})$ are the rotation matrices corresponding to $\mathbf{q}$ and $\mathbf{s}$, respectively.

The global, IMU, and the camera frames are denoted by $\{G\}$, $\{I\}$, and $\{C\}$, respectively.

The skew-symmetric matrix of vector $\mathbf{a}$ is represented by $\lfloor\mathbf{a}\rfloor$, and the following properties of the cross product skew-symmetric matrix are used: $\mathbf{a}\times\mathbf{b} = \lfloor\mathbf{a}\rfloor\mathbf{b} = -\lfloor\mathbf{b}\rfloor\mathbf{a}$, $\lfloor\mathbf{a}\rfloor\mathbf{a} = \mathbf{0}_{3\times 1}$, $\lfloor\mathbf{a}\rfloor\lfloor\mathbf{b}\rfloor = \mathbf{b}\mathbf{a}^\top - (\mathbf{a}^\top\mathbf{b})\mathbf{I}_3$, $\lfloor\mathbf{A}\mathbf{b}\rfloor = \mathbf{A}\lfloor\mathbf{b}\rfloor\mathbf{A}^\top$, $\mathbf{b}^\top\lfloor\mathbf{a}\rfloor\mathbf{b} = 0$, $\forall\ \mathbf{A} \in \mathbb{R}^{3\times 3}$ and $\forall\ \{\mathbf{a},\mathbf{b}\} \in \mathbb{R}^{3\times 1}$.

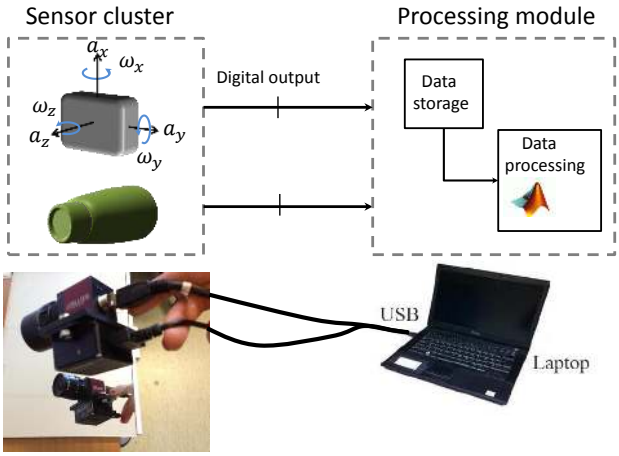

Fig. 2: Overall system architecture. The sensor module, consisting of an IMU (three orthogonal accelerometers and three orthogonal gyroscopes) that is rigidly mounted to a monocular camera. The stored measurements are processed by a laptop to perform state estimation in the processing platform.

III. System Description

In this section, we present the general system description. First, the experimental setup is introduced. Then, the IMU-camera process model and the camera measurement model are described. These models are later used for analyzing the observability properties and for state estimation of the calibration parameters in the proposed system.

A. Experimental setup

The hardware of our visual inertial system consists of a monocular camera—as a vision sensor—that is rigidly mounted on an IMU—as an inertial sensor.

For the experiments, we used a MicroStrain 3DMGX2 IMU with sampling rate of 250 Hz, which was rigidly mounted on

an internally calibrated AVT Guppy monocular camera with a resolution of 752×480 pixels and a sampling rate of 10 Hz.

Fig. 2 provides a general overview of the system architecture. The IMU sensor unit and the camera are shown on the left-hand side. The sensor module is directly connected to a laptop via a USB port. The measurements are first stored in the processing platform, and then the estimation is done off-line in MATLAB.

For estimating the 6-DoF rigid body transformation between the camera and the IMU, we propose an approach based on an IMU-camera *ego-motion* estimation method. During calibration, we assume that the IMU-camera is navigating in front of a planar mirror, which is horizontally or vertically aligned. We formulate the problem in a state-space model and use an unscented Kalman filter for state estimation. In the model, the IMU measurements (linear acceleration and rotational velocity) with higher rates are used for state propagation, and the camera measurements with lower rates are used for state correction. The visual corrections are obtained from the positions of the key features' reflections in the 2D image plane, which are tracked between image frames. The key features are located arbitrarily (without any prior assumption on their 3D positions with respect to the camera) on the camera body, such that their reflections in the mirror are in the camera's field of view. Fig. 1 illustrates a potential application of the mirror-based IMU-camera calibration procedure for a smartphone. The logo of the phone can be considered as an object whose features' reflections in the mirror are in the camera's field of view.

B. Propagation model

We solve the problem of IMU-camera calibration through a navigation system in which the camera observes the reflections of a set of key features in the mirror. Thus, we consider the system state variables to be:[1] 1) motion parameters of the sensors (rotation, velocity, position) in the global reference frame, 2) IMU-camera calibration parameters, 3) the 3D positions of the key features with respect to the camera[2]. The total system state vector is

$$\mathbf{x} = \begin{bmatrix} {}^{I}\mathbf{s}_G{}^{\top} & {}^{G}\mathbf{v}_I{}^{\top} & {}^{G}\mathbf{p}_I{}^{\top} & {}^{C}\mathbf{s}_I{}^{\top} & {}^{I}\mathbf{p}_C{}^{\top} & {}^{C}\mathbf{p}_{f_1}{}^{\top} & \cdots & {}^{C}\mathbf{p}_{f_M}{}^{\top} \end{bmatrix}^{\top}, \quad (1)$$

where ${}^{I}\mathbf{s}_G$ represents the orientation of the global frame $\{G\}$ in the IMU's frame of reference $\{I\}$, ${}^{G}\mathbf{v}_I$ and ${}^{G}\mathbf{p}_I$ denote the velocity and position of $\{I\}$ in $\{G\}$, respectively; ${}^{C}\mathbf{s}_I$ represents the rotation of the IMU in the camera frame, ${}^{I}\mathbf{p}_C$ is the position of $\{C\}$ in $\{I\}$, and ${}^{C}\mathbf{p}_{f_k}$ for $k \in \{1,...,M\}$ is the position of the k-th key feature in the camera's frame of reference.

The following describes the time evolution of our visual inertial system:

$$\begin{aligned} {}^{I}\dot{\mathbf{s}}_G(t) &= \frac{1}{2}\mathbf{D}\ {}^{I}\omega(t), \\ {}^{G}\dot{\mathbf{v}}_I(t) &= {}^{G}\mathbf{a}(t) = {}^{G}\mathbf{g} + \mathbf{C}({}^{I}\mathbf{s}_G(t))^{\top}{}^{I}\mathbf{a}(t), \\ {}^{G}\dot{\mathbf{p}}_I(t) &= {}^{G}\mathbf{v}_I(t), \qquad {}^{C}\dot{\mathbf{s}}_I(t) = \mathbf{0}_{3\times 1}, \qquad {}^{I}\dot{\mathbf{p}}_C(t) = \mathbf{0}_{3\times 1}, \\ {}^{C}\dot{\mathbf{p}}_{f_k}(t) &= \mathbf{0}_{3\times 1} \quad \text{for} \quad k \in \{1,...,M\}, \end{aligned} \quad (2)$$

where $\frac{1}{2}\mathbf{D} \triangleq \frac{\partial {}^{I}\mathbf{s}_G}{\partial {}^{I}\theta_G} = \frac{1}{2}(\mathbf{I}_3 + \lfloor {}^{I}\mathbf{s}_G \rfloor + {}^{I}\mathbf{s}_G\ {}^{I}\mathbf{s}_G{}^{\top})$, and where ${}^{I}\omega(t) = \begin{bmatrix}\omega_1 & \omega_2 & \omega_3\end{bmatrix}^{\top}$ and ${}^{I}\mathbf{a}(t) = \begin{bmatrix}a_1 & a_2 & a_3\end{bmatrix}^{\top}$ are the rotational velocities and linear accelerations, respectively, expressed in $\{I\}$; ${}^{G}\mathbf{g} = \begin{bmatrix}0 & 0 & g\end{bmatrix}^{\top}$ is the gravitational acceleration, and $\mathbf{C}({}^{I}\mathbf{s}_G(t))$ is the rotation matrix corresponding to ${}^{I}\mathbf{s}_G$.

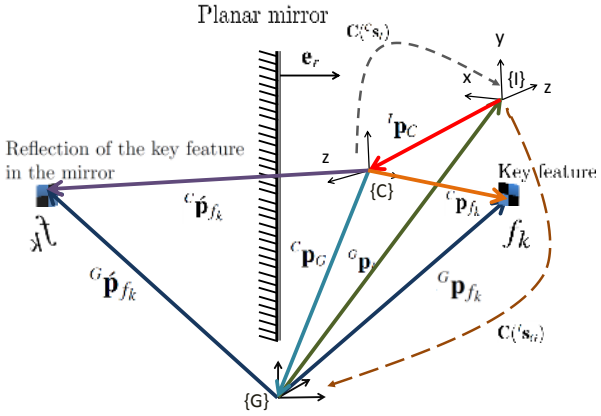

Fig. 3: Geometrical relation between the IMU, camera, and global coordinate frames and the position of a key feature f_k and its reflection in the mirror. The relative IMU-camera rotation and translation are denoted as $\mathbf{C}({}^{C}\mathbf{s}_I)$ and ${}^{I}\mathbf{p}_C$, respectively. Feature f_k is assumed to be rigidly attached to the IMU and camera frame of reference where its reflection in the mirror is in the camera's field of view. $\mathbf{e}_r$ is the normal of the mirror.

C. Measurement model

The camera measures the perspective projection of 3D points, expressed in the camera coordinate frame, onto the image plane. In our setup, the camera captures images in front of a planar mirror and we are only interested in the perspective projection of *virtual features* (the reflection of real features in the mirror) in the image. More specifically, we consider a set of key features rigidly attached to the IMU-camera body, and track their corresponding virtual features in the images.

Assuming a calibrated pinhole camera, the camera measurements from the virtual features in normalized pixel coordinates can be expressed as

$$\mathbf{z}_k = \begin{bmatrix} u_k \\ v_k \\ 1 \end{bmatrix} = \frac{1}{\mathbf{e}_3^{\top}{}^{C}\acute{\mathbf{p}}_{f_k}}{}^{C}\acute{\mathbf{p}}_{f_k}, \quad (3)$$

where ${}^{C}\acute{\mathbf{p}}_{f_k}$ represents the 3D position of the k-th virtual feature with respect to the camera.

Lemma 1. *Let us consider a planar mirror, which is horizontally or vertically aligned with respect to the global coordinate*

[1] For the sake of simplicity, we ignore the biases in the IMU measurement for our analysis. However, they are considered for the state estimation in Section V.

[2] In Section IV-B1, we prove that the IMU-camera's external calibration parameters are observable using only two features. But for now, we consider M key features in the state vector.

frame. This implies that the normal of the mirror plane is $\mathbf{e}_r$ *where, depending on the mirror's alignment,* $r \in \{1,2,3\}$. *Then the 3D position of the virtual key feature* f_k *in the camera coordinate frame,* ${}^C\acute{\mathbf{p}}_{f_k}$, *as a function of the state variables, can be described as*

$$ {}^C\acute{\mathbf{p}}_{f_k} = {}^C\mathbf{p}_{f_k} - 2\mathbf{C}_C\mathbf{C}\mathbf{e}_r\mathbf{e}_r^\top \left(\mathbf{C}^\top\mathbf{C}_C^\top {}^C\mathbf{p}_{f_k} + {}^G\mathbf{p}_I + \mathbf{C}^\top {}^I\mathbf{p}_C\right), \quad (4) $$

where $\mathbf{C} \triangleq \mathbf{C}({}^I\mathbf{s}_G)$ *and* $\mathbf{C}_C \triangleq \mathbf{C}({}^C\mathbf{s}_I)$.

Proof: Depending on the alignment of the mirror (horizontally or vertically), we define the reflection matrix $\mathbf{A}_r$ that relates the 3D coordinates of the real and virtual features in the global frame as

$$ {}^G\acute{\mathbf{p}}_{f_k} = \mathbf{A}_r {}^G\mathbf{p}_{f_k}, \quad (5) $$

where

$$ \mathbf{A}_r = \mathbf{I}_3 - 2\mathbf{e}_r\mathbf{e}_r^\top, \quad (6) $$

and where ${}^G\mathbf{p}_{f_k}$ and ${}^G\acute{\mathbf{p}}_{f_k}$ are the positions of the k-th real and virtual features in the global frame of reference, respectively; see Fig. 3. $\mathbf{e}_r$ is the normal of the mirror in the global frame of reference. That is, depending on the alignment of the mirror it can be $\mathbf{e}_1$, $\mathbf{e}_2$, or $\mathbf{e}_3$. The geometrical relation between different coordinate frames and the position vectors are presented in Fig. 3.

Moreover, the geometric relation between ${}^C\acute{\mathbf{p}}_{f_k}$ and ${}^G\acute{\mathbf{p}}_{f_k}$ (as follows from Fig. 3) is described as

$$ {}^C\acute{\mathbf{p}}_{f_k} = \mathbf{C}_C\mathbf{C}{}^G\acute{\mathbf{p}}_{f_k} + {}^C\mathbf{p}_G, \quad (7) $$

where

$$ {}^C\mathbf{p}_G = -\mathbf{C}_C\mathbf{C}{}^G\mathbf{p}_I - \mathbf{C}_c\,{}^I\mathbf{p}_C. \quad (8) $$

Accordingly, ${}^C\mathbf{p}_{f_k}$ and ${}^G\mathbf{p}_{f_k}$ are related by

$$ {}^C\mathbf{p}_{f_k} = \mathbf{C}_C\mathbf{C}{}^G\mathbf{p}_{f_k} + {}^C\mathbf{p}_G, \quad (9) $$

$$ \Rightarrow {}^G\mathbf{p}_{f_k} = \mathbf{C}^\top\mathbf{C}_C^\top \left({}^C\mathbf{p}_{f_k} - {}^C\mathbf{p}_G\right). \quad (10) $$

By substituting (10) and (5) in (7), we have

$$ \begin{aligned} {}^C\acute{\mathbf{p}}_{f_k} &= \mathbf{C}_C\mathbf{C}\mathbf{A}\mathbf{C}^\top\mathbf{C}_C^\top \left({}^C\mathbf{p}_{f_k} - {}^C\mathbf{p}_G\right) + {}^C\mathbf{p}_G \quad (11)\\ &= {}^C\mathbf{p}_{f_k} - 2\mathbf{C}_C\mathbf{C}\mathbf{e}_r\mathbf{e}_r^\top {}^C\mathbf{p}_{f_k} + \\ &\quad \left(-\mathbf{C}_C\mathbf{C}\mathbf{A}\mathbf{C}^\top\mathbf{C}_C^\top + \mathbf{I}_3\right){}^C\mathbf{p}_G \\ &= {}^C\mathbf{p}_{f_k} - 2\mathbf{C}_C\mathbf{C}\mathbf{e}_r\mathbf{e}_r^\top\mathbf{C}^\top\mathbf{C}_C^\top {}^C\mathbf{p}_{f_k} + \\ &\quad 2\mathbf{C}_C\mathbf{C}\mathbf{e}_r\mathbf{e}_r^\top\mathbf{C}^\top\mathbf{C}_C^\top {}^C\mathbf{p}_G. \end{aligned} $$

Finally, by substituting (8) in (11) we get

$$ \begin{aligned} {}^C\acute{\mathbf{p}}_{f_k} &= {}^C\mathbf{p}_{f_k} - 2\mathbf{C}_C\mathbf{C}\mathbf{e}_r\mathbf{e}_r^\top\mathbf{C}^\top\mathbf{C}_C^\top {}^C\mathbf{p}_{f_k} - \quad (12)\\ &\quad 2\mathbf{C}_C\mathbf{C}\mathbf{e}_r\mathbf{e}_r^\top {}^I\mathbf{p}_G - 2\mathbf{C}_C\mathbf{C}\mathbf{e}_r\mathbf{e}_r^\top\mathbf{C}^\top {}^I\mathbf{p}_C \\ &= {}^C\mathbf{p}_{f_k} - 2\mathbf{C}_C\mathbf{C}\mathbf{e}_r\mathbf{e}_r^\top \left(\mathbf{C}^\top\mathbf{C}_C^\top {}^C\mathbf{p}_{f_k} + {}^G\mathbf{p}_I + \mathbf{C}^\top {}^I\mathbf{p}_C\right). \end{aligned} $$

■

Lemma 1 shows that the measurement model (3) can be explicitly written as a nonlinear function of the state variables. Thus, the estimation of the state variables can now be performed by using the unscented Kalman filter (Section V).

IV. Nonlinear Observability Analysis

Observability provides an understanding of how well states of a system can be inferred from the system output measurements. For an observable system, we can determine the behavior of the entire system from the system measurements. For an unobservable system, the current values of some of its states cannot be determined from system output measurements. The observability properties of a time invariant linear system can be easily derived using the Kalman canonical decomposition. However, the problem becomes more complex for a nonlinear system, such as for the IMU-camera calibration. In this case, the study of observability properties is restricted to a local weak observability analysis [25], which focuses on distinguishability.

One way to study the observability properties of nonlinear systems is by analyzing the rank condition of its observability matrix, which is constructed from the span of the system's Lie derivatives [25].

Similar to [14], [16], [18], our observability analysis for the IMU-camera calibration is based on the Lie derivatives. However, instead of using an inferred camera measurement model or pseudo measurements like in [14] and [16], we analyze the original system measurement equation, which is a more difficult problem.

In the following, we first provide an overview of the observability rank condition test [25]. Then, we briefly describe the approach in [18], which assists the process of finding the unobservable states when using the Lie derivatives rank condition test. Finally, we perform our analysis that is based on [18].

A. Observability rank condition with the Lie derivative

Consider a nonlinear system

$$ \begin{cases} \dot{\mathbf{x}} = \mathbf{f}_0(\mathbf{x}) + \sum_{i=1}^{\ell} \mathbf{f}_i(\mathbf{x})u_i \\ \mathbf{y} = \mathbf{h}(\mathbf{x}) \end{cases} \quad (13) $$

where $\mathbf{x} \in \mathbb{R}^m$ is the state vector, $\mathbf{u} = [u_1 \cdots u_\ell]^\top \in \mathbb{R}^\ell$ is the system input, $\mathbf{y} \in \mathbb{R}^k$ is the system output, and $\mathbf{f}_i$ for $i \in \{0,\ldots,\ell\}$ is the process function.

For the *input-linear* system (13), we now provide the required rules for calculating the Lie derivatives to construct the observability matrix.

The zeroth order Lie derivative of a measurement function $\mathbf{h}$ is the function itself, i.e.,

$$ \mathfrak{L}^0\mathbf{h} = \mathbf{h}(\mathbf{x}). \quad (14) $$

For any n-th order Lie derivative, $\mathfrak{L}^n\mathbf{h}$, the $n+1$-th order Lie derivative $\mathfrak{L}^{n+1}_{\mathbf{f}_i}\mathbf{h}$, with respect to a process function $\mathbf{f}_i$ can be computed as

$$ \mathfrak{L}^{n+1}_{\mathbf{f}_i}\mathbf{h} = \nabla\mathfrak{L}^n\mathbf{h}\cdot\mathbf{f}_i, \quad (15) $$

where ∇ denotes the gradient operator with respect to $\mathbf{x}$ and '$\cdot$' represents the vector inner product. Similarly, mixed higher order Lie derivatives can be defined as

$$ \mathfrak{L}^n_{\mathbf{f}_i\mathbf{f}_{j\ldots}\mathbf{f}_d}\mathbf{h} = \mathfrak{L}_{\mathbf{f}_i}(\mathfrak{L}^{n-1}_{\mathbf{f}_{j\ldots}\mathbf{f}_d}\mathbf{h}) = \nabla\mathfrak{L}^{n-1}_{\mathbf{f}_{j\ldots}\mathbf{f}_d}\mathbf{h}\cdot\mathbf{f}_i, \quad (16) $$

where $i,j,d \in \{0,\ldots,\ell\}$.

The observability of a system is determined by calculating the dimension of the space spanned by the gradients of the Lie derivatives of its output functions [25]. Hence, the observability matrix $\mathbf{O}$ for system (13) is defined as

$$\mathbf{O} \triangleq \begin{bmatrix} \nabla \mathfrak{L}^0 \mathbf{h} \\ \nabla \mathfrak{L}^1_{\mathbf{f}_i} \mathbf{h} \\ \vdots \\ \nabla \mathfrak{L}^n_{\mathbf{f}_i \mathbf{f}_j \dots \mathbf{f}_d} \mathbf{h} \\ \vdots \end{bmatrix}. \tag{17}$$

To prove that a system is observable, it is sufficient to show that $\mathbf{O}$ is of full column rank. For an unobservable system, the null vectors of $\mathbf{O}$ span the system's unobservable subspace. Hence, to find the unobservable subspace, we have to find the null space of matrix $\mathbf{O}$, where $\mathbf{O}$ may have infinitely many rows. This can be a very challenging and difficult task, especially for high-dimensional systems. One way to address this issue is to decompose the infinite dimensional matrix $\mathbf{O}$ into $\mathbf{O} = \Xi\Omega$, where Ξ is infinitely dimensional as $\mathbf{O}$, but Ω has finite dimension. If we can show that Ξ is of full column rank, then the null space of Ω will span the unobservable directions of $\mathbf{O}$.

For the analysis, we use Theorem 1 in [18], which is summarized in the following:

Theorem 1. *Assume that there exists a nonlinear transformation $\beta(\mathbf{x}) = [\beta_1(\mathbf{x})^\top \dots \beta_n(\mathbf{x})^\top]^\top$ (i.e., a set of basis functions) of the variable $\mathbf{x}$, such that:*

1) *The system measurement equation can be written as a function of β, i.e., $\mathbf{y} = \mathbf{h}(\mathbf{x}) = \overline{\mathbf{h}}(\beta)$*
2) *$\frac{\partial \beta}{\partial \mathbf{x}} \mathbf{f}_j$, for $j = \{0, \dots, \ell\}$ is a function of β*

Then,

- *the observability matrix of system* (13) *can be factorized as $\mathbf{O} = \Xi\Omega$, where Ξ is the observability matrix of the system*

$$\begin{cases} \dot{\beta} = \mathbf{g}_0(\beta) + \sum_{i=1}^{\ell} \mathbf{g}_i(\beta) u_i \\ \mathbf{y} = \overline{\mathbf{h}}(\beta) \end{cases}, \tag{18}$$

  and $\Omega \triangleq \frac{\partial \beta}{\partial \mathbf{x}}$.
- *if Ξ is of full column rank, i.e., system* (18) *is observable, then the unobservable directions of system* (13) *will be spanned by the null vectors of Ω.*

Using Theorem 1, we perform the observability analysis for our proposed IMU-camera system in the following subsection.

B. Observability properties of the proposed system

For the observability analysis, we first rewrite the system model (2) in the form of the input-linear system (13)

$$\begin{bmatrix} {}^I\dot{\mathbf{s}}_G \\ {}^G\dot{\mathbf{v}}_I \\ {}^G\dot{\mathbf{p}}_I \\ {}^C\dot{\mathbf{s}}_I \\ {}^I\dot{\mathbf{p}}_C \\ {}^C\dot{\mathbf{p}}_{f_1} \\ \vdots \\ {}^C\dot{\mathbf{p}}_{f_M} \end{bmatrix} = \underbrace{\begin{bmatrix} \mathbf{0}_{3\times1} \\ \mathbf{g} \\ {}^G\mathbf{v}_I \\ \mathbf{0}_{3\times1} \\ \mathbf{0}_{3\times1} \\ \mathbf{0}_{3\times1} \\ \vdots \\ \mathbf{0}_{3\times1} \end{bmatrix}}_{\mathbf{f}_0} + \underbrace{\begin{bmatrix} \frac{1}{2}\mathbf{D} \\ \mathbf{0}_{3\times3} \\ \mathbf{0}_{3\times3} \\ \mathbf{0}_{3\times3} \\ \mathbf{0}_{3\times3} \\ \mathbf{0}_{3\times3} \\ \vdots \\ \mathbf{0}_{3\times3} \end{bmatrix}}_{\mathbf{F}_1} \omega + \underbrace{\begin{bmatrix} \mathbf{0}_{3\times3} \\ \mathbf{C}^\top \\ \mathbf{0}_{3\times3} \\ \mathbf{0}_{3\times3} \\ \mathbf{0}_{3\times3} \\ \mathbf{0}_{3\times3} \\ \vdots \\ \mathbf{0}_{3\times3} \end{bmatrix}}_{\mathbf{F}_2} \mathbf{a}, \tag{19}$$

where $\mathbf{f}_0 \in \mathbb{R}^{15+3M}$, $\mathbf{F}_1 \in \mathbb{R}^{(15+3M)\times3}$ and $\mathbf{F}_2 \in \mathbb{R}^{(15+3M)\times3}$ represent three process functions as

$$\begin{aligned} \mathbf{F}_1\omega &= \mathbf{f}_{11}\omega_1 + \mathbf{f}_{12}\omega_2 + \mathbf{f}_{13}\omega_3, \\ \mathbf{F}_2\mathbf{a} &= \mathbf{f}_{21}a_1 + \mathbf{f}_{22}a_2 + \mathbf{f}_{23}a_3. \end{aligned} \tag{20}$$

To perform the observability analysis, we consider the camera measurement model (3) in the form of

$$(\mathbf{z}\mathbf{e}_3^\top - \mathbf{I}_3)\,{}^C\acute{\mathbf{p}}_f = \mathbf{T}\ {}^C\acute{\mathbf{p}}_f = \mathbf{0}_{3\times1}, \tag{21}$$

where $\mathbf{T} \triangleq (\mathbf{z}\mathbf{e}_3^\top - \mathbf{I}_3)$. Then we redefine the system measurement model for the k-th key feature (by substituting (4) into (21)) as

$$\begin{aligned} \mathbf{y}_k &= \mathbf{h}_k(\mathbf{x}) = \mathbf{T}_k\,{}^C\acute{\mathbf{p}}_{f_k} \\ &= \mathbf{T}_k \left({}^C\mathbf{p}_{f_k} - 2\mathbf{C}_C\mathbf{C}\mathbf{e}_r\mathbf{e}_r^\top \left(\mathbf{C}^\top \mathbf{C}_C^\top\, {}^C\mathbf{p}_{f_k} + {}^G\mathbf{p}_I + \mathbf{C}^\top\, {}^I\mathbf{p}_C \right) \right). \end{aligned} \tag{22}$$

To define the basis functions, we start with the system measurement equation (22) for the k-th feature (first condition of Theorem 1). We define initial basis functions from the unknown terms appearing in the measurement function (22) as

$$\begin{aligned} \beta_{1k} &= {}^C\mathbf{p}_{f_k}, & \beta_2 &= \mathbf{C}_C\mathbf{C}\mathbf{e}_r, \\ \beta_3 &= \mathbf{e}_r^\top\, {}^G\mathbf{p}_I, & \beta_4 &= {}^C\mathbf{s}_I, & \beta_5 &= {}^I\mathbf{p}_C. \end{aligned} \tag{23}$$

To check the second condition of Theorem 1, we compute derivatives of the defined bases with respect to the state vector $\mathbf{x}$, as

$$\frac{\partial \beta_{1k}}{\partial \mathbf{x}} = \begin{bmatrix} \mathbf{0}_{3\times3} & \mathbf{0}_{3\times3} & \mathbf{0}_{3\times3} & \mathbf{0}_{3\times3} & \mathbf{0}_{3\times3} & \mathbf{0}_{3\times3(k-1)} & \mathbf{I}_3 & \mathbf{0}_{3\times3(M-k-1)} \end{bmatrix}, \tag{24}$$

$$\frac{\partial \beta_2}{\partial \mathbf{x}} = \begin{bmatrix} \mathbf{C}_C \lfloor \mathbf{C}\mathbf{e}_r \rfloor \frac{\partial {}^I\theta_G}{\partial {}^I\mathbf{s}_G} & \mathbf{0}_{3\times3} & \mathbf{0}_{3\times3} & \lfloor \mathbf{C}_C\mathbf{C}\mathbf{e}_r \rfloor \frac{\partial {}^C\theta_I}{\partial {}^C\mathbf{s}_I} & \mathbf{0}_{3\times3M} \end{bmatrix}, \tag{25}$$

$$\frac{\partial \beta_3}{\partial \mathbf{x}} = \begin{bmatrix} \mathbf{0}_{1\times3} & \mathbf{0}_{1\times3} & \mathbf{e}_r^\top & \mathbf{0}_{1\times3} & \mathbf{0}_{1\times3} & \mathbf{0}_{1\times3M} \end{bmatrix}, \tag{26}$$

$$\frac{\partial \beta_4}{\partial \mathbf{x}} = \begin{bmatrix} \mathbf{0}_{3\times3} & \mathbf{0}_{3\times3} & \mathbf{0}_{3\times3} & \mathbf{I}_3 & \mathbf{0}_{3\times3} & \mathbf{0}_{3\times3M} \end{bmatrix}, \tag{27}$$

$$\frac{\partial \beta_5}{\partial \mathbf{x}} = \begin{bmatrix} \mathbf{0}_{3\times3} & \mathbf{0}_{3\times3} & \mathbf{0}_{3\times3} & \mathbf{0}_{3\times3} & \mathbf{I}_3 & \mathbf{0}_{3\times3M} \end{bmatrix}, \tag{28}$$

and project them onto all the process functions. Starting from $\beta_{1k} \triangleq {}^C\mathbf{p}_{f_k}$, we have

$$\frac{\partial \beta_{1k}}{\partial \mathbf{x}} \mathbf{f}_0 = \mathbf{0}_{3\times1}, \quad \frac{\partial \beta_{1k}}{\partial \mathbf{x}} \mathbf{f}_{1i} = \mathbf{0}_{3\times1}, \quad \frac{\partial \beta_{1k}}{\partial \mathbf{x}} \mathbf{f}_{2i} = \mathbf{0}_{3\times1}, \tag{29}$$

for $i=\{1,2,3\}$. Following the same process, for the span of $\beta_2 \triangleq \mathbf{C}_C\mathbf{C}\mathbf{e}_r$, we have

$$\begin{aligned}\frac{\partial \beta_2}{\partial \mathbf{x}}\mathbf{f}_0 &= \mathbf{0}_{3\times 1},\\ \frac{\partial \beta_2}{\partial \mathbf{x}}\mathbf{f}_{1i} &= \mathbf{C}_C\lfloor \mathbf{C}\mathbf{e}_r\rfloor \mathbf{e}_i,\\ &= \lfloor \mathbf{C}_C\mathbf{C}\mathbf{e}_r\rfloor \mathbf{C}_C\mathbf{e}_i = \lfloor \beta_2\rfloor \mathbf{C}(\beta_4)\mathbf{e}_i,\\ \frac{\partial \beta_2}{\partial \mathbf{x}}\mathbf{f}_{2i} &= \mathbf{0}_{3\times 1}.\end{aligned} \tag{30}$$

For the span of $\beta_3 \triangleq \mathbf{e}_r^{\top I}\mathbf{p}_G$:

$$\frac{\partial \beta_3}{\partial \mathbf{x}}\mathbf{f}_0 = \mathbf{e}_r^{\top G}\mathbf{v}_I \triangleq \beta_6, \quad \frac{\partial \beta_3}{\partial \mathbf{x}}\mathbf{f}_{1i} = 0, \quad \frac{\partial \beta_3}{\partial \mathbf{x}}\mathbf{f}_{2i} = 0, \tag{31}$$

where $\beta_6 \triangleq \mathbf{e}_r^{\top G}\mathbf{v}_I$ is a newly defined basis function.

Then the span of $\beta_4 \triangleq {}^C\mathbf{s}_I$:

$$\frac{\partial \beta_4}{\partial \mathbf{x}}\mathbf{f}_0 = \mathbf{0}_{3\times 1}, \quad \frac{\partial \beta_4}{\partial \mathbf{x}}\mathbf{f}_{1i} = \mathbf{0}_{3\times 1}, \quad \frac{\partial \beta_4}{\partial \mathbf{x}}\mathbf{f}_{2i} = \mathbf{0}_{3\times 1}. \tag{32}$$

Finally, for $\beta_5 \triangleq {}^I\mathbf{p}_C$, we get

$$\frac{\partial \beta_5}{\partial \mathbf{x}}\mathbf{f}_0 = \mathbf{0}_{3\times 1}, \quad \frac{\partial \beta_5}{\partial \mathbf{x}}\mathbf{f}_{1i} = \mathbf{0}_{3\times 1}, \quad \frac{\partial \beta_5}{\partial \mathbf{x}}\mathbf{f}_{2i} = \mathbf{0}_{3\times 1}. \tag{33}$$

In the next step, we proceed to find the derivative of the newly defined basis function $\beta_6 \triangleq \mathbf{e}_r^{\top G}\mathbf{v}_I$ with respect to the state vector $\mathbf{x}$

$$\frac{\partial \beta_3}{\partial \mathbf{x}} = \begin{bmatrix}\mathbf{0}_{1\times 3} & \mathbf{e}_r^{\top} & \mathbf{0}_{1\times 3} & \mathbf{0}_{1\times 3} & \mathbf{0}_{1\times 3} & \mathbf{0}_{1\times 3M}\end{bmatrix}, \tag{34}$$

and calculate its projection onto all the process functions as

$$\begin{aligned}\frac{\partial \beta_6}{\partial \mathbf{x}}\mathbf{f}_0 &= \mathbf{e}_r^{\top}\mathbf{g} = g, \quad \frac{\partial \beta_6}{\partial \mathbf{x}}\mathbf{f}_{1i} = 0,\\ \frac{\partial \beta_6}{\partial \mathbf{x}}\mathbf{f}_{2i} &= \mathbf{e}_r^{\top}\mathbf{C}^{\top}\mathbf{e}_i = \mathbf{e}_r^{\top}\mathbf{C}^{\top}\mathbf{C}_C^{\top}\mathbf{C}_C\mathbf{e}_i = \beta_2^{\top}\mathbf{C}(\beta_4)\mathbf{e}_i.\end{aligned} \tag{35}$$

Since all the terms in the preceding projections are defined based on the existing basis functions (i.e., second condition of Theorem 1 is satisfied), we terminate the process of defining new basis functions. This means that we have found all the complete bases. Thus, the corresponding new process model for the defined bases can be written as

$$\begin{bmatrix}\dot\beta_{11}\\ \vdots\\ \dot\beta_{1M}\\ \dot\beta_2\\ \dot\beta_3\\ \dot\beta_4\\ \dot\beta_5\\ \dot\beta_6\end{bmatrix} = \underbrace{\begin{bmatrix}\mathbf{0}_{3\times 1}\\ \vdots\\ \mathbf{0}_{3\times 1}\\ \mathbf{0}_{3\times 1}\\ \beta_6\\ \mathbf{0}_{3\times 1}\\ \mathbf{0}_{3\times 1}\\ g\end{bmatrix}}_{\mathbf{g}_0} + \underbrace{\begin{bmatrix}\mathbf{0}_{3\times 3}\\ \vdots\\ \mathbf{0}_{3\times 3}\\ \lfloor\beta_2\rfloor\mathbf{C}(\beta_4)\\ \mathbf{0}_{1\times 3}\\ \mathbf{0}_{3\times 3}\\ \mathbf{0}_{3\times 3}\\ \mathbf{0}_{1\times 3}\end{bmatrix}}_{\mathbf{G}_1}\omega + \underbrace{\begin{bmatrix}\mathbf{0}_{3\times 3}\\ \vdots\\ \mathbf{0}_{3\times 3}\\ \mathbf{0}_{3\times 3}\\ \mathbf{0}_{1\times 3}\\ \mathbf{0}_{3\times 3}\\ \mathbf{0}_{3\times 3}\\ \beta_2^{\top}\mathbf{C}(\beta_4)\end{bmatrix}}_{\mathbf{G}_2}\mathbf{a}, \tag{36}$$

and the measurement equation in terms of the basis functions for the k-th key feature is

$$\mathbf{y}_k(\beta) = \bar{\mathbf{h}}_k(\beta) = \mathbf{T}_k(\beta_{1k} - 2\beta_2\beta_2^{\top}\beta_1 - 2\beta_2\beta_3 - \beta_2\beta_2^{\top}\mathbf{C}(\beta_4)\beta_5). \tag{37}$$

1) Rank condition test for Ξ: We study the observability of system (36) using the algebraic test. For this purpose, we first need to derive the gradients of the Lie derivatives of the measurement functions. To prove that matrix Ξ is a full column rank matrix, it suffices to show that a subset of its rows, whose dimension is the same or larger than the number of columns, is linearly independent.

To show that Ξ is of full column rank, we form matrix $\bar\Xi$ that is a sub-matrix of Ξ with the following Lie derivative gradients for the two measurement functions $\bar{\mathbf{h}}_1$ and $\bar{\mathbf{h}}_2$:[3]

$$\begin{aligned}&\{\nabla\mathfrak{L}^0\bar{\mathbf{h}}_1, \nabla\mathfrak{L}^0\bar{\mathbf{h}}_2, \nabla\mathfrak{L}^1_{\mathbf{g}_0}\bar{\mathbf{h}}_1, \nabla\mathfrak{L}^1_{\mathbf{g}_{11}}\bar{\mathbf{h}}_1, \nabla\mathfrak{L}^1_{\mathbf{g}_{12}}\bar{\mathbf{h}}_1, \nabla\mathfrak{L}^1_{\mathbf{g}_{13}}\bar{\mathbf{h}}_1, \nabla\mathfrak{L}^1_{\mathbf{g}_{11}}\bar{\mathbf{h}}_2,\\ &\nabla\mathfrak{L}^1_{\mathbf{g}_{12}}\bar{\mathbf{h}}_2, \nabla\mathfrak{L}^1_{\mathbf{g}_{13}}\bar{\mathbf{h}}_2, \nabla\mathfrak{L}^2_{\mathbf{g}_0\mathbf{g}_{11}}\bar{\mathbf{h}}_1, \nabla\mathfrak{L}^2_{\mathbf{g}_0\mathbf{g}_{12}}\bar{\mathbf{h}}_1, \nabla\mathfrak{L}^2_{\mathbf{g}_0\mathbf{g}_{13}}\bar{\mathbf{h}}_1, \nabla\mathfrak{L}^2_{\mathbf{g}_0\mathbf{g}_{21}}\bar{\mathbf{h}}_1,\\ &\nabla\mathfrak{L}^2_{\mathbf{g}_0\mathbf{g}_{22}}\bar{\mathbf{h}}_1, \nabla\mathfrak{L}^2_{\mathbf{g}_0\mathbf{g}_{23}}\bar{\mathbf{h}}_1, \nabla\mathfrak{L}^2_{\mathbf{g}_{11}\mathbf{g}_{11}}\bar{\mathbf{h}}_1, \nabla\mathfrak{L}^2_{\mathbf{g}_{12}\mathbf{g}_{12}}\bar{\mathbf{h}}_1, \nabla\mathfrak{L}^2_{\mathbf{g}_{13}\mathbf{g}_{13}}\bar{\mathbf{h}}_1\}.\end{aligned} \tag{38}$$

In APPENDIX A, we derive the explicit expressions for the Lie derivatives and their corresponding gradients to construct $\bar\Xi$. In APPENDIX B, we prove that $\bar\Xi$ is of full column rank if $\beta_6 \neq 0$ ($\mathbf{e}_r^{\top G}\mathbf{v}_I \neq 0$). Then by performing Gaussian elimination in $\bar\Xi$, we get:

$$\begin{bmatrix}\mathbf{0}_{3\times 3} & \mathbf{0}_{3\times 3} & \mathbf{0}_{3\times 3} & \mathbf{0}_{3\times 1} & \mathbf{0}_{3\times 3} & \mathbf{I}_3 & \mathbf{0}_{3\times 1}\\ \mathbf{0}_{1\times 3} & \mathbf{0}_{1\times 3} & \mathbf{0}_{1\times 3} & \mathbf{0}_{1\times 3} & \mathbf{0}_{1\times 3} & \mathbf{0}_{1\times 3} & 1\\ \mathbf{I}_3 & \mathbf{0}_{3\times 3} & \mathbf{0}_{3\times 3} & \mathbf{0}_{3\times 1} & \mathbf{0}_{3\times 3} & \mathbf{0}_{3\times 3} & \mathbf{0}_{3\times 1}\\ \mathbf{0}_{3\times 3} & \mathbf{I}_3 & \mathbf{0}_{3\times 3} & \mathbf{0}_{3\times 1} & \mathbf{0}_{3\times 3} & \mathbf{0}_{3\times 3} & \mathbf{0}_{3\times 1}\\ \mathbf{0}_{3\times 3} & \mathbf{0}_{3\times 3} & \mathbf{0}_{3\times 3} & \mathbf{0}_{3\times 1} & \mathbf{I}_3 & \mathbf{0}_{3\times 3} & \mathbf{0}_{3\times 1}\\ \mathbf{0}_{3\times 3} & \mathbf{0}_{3\times 3} & \mathbf{I}_3 & \mathbf{0}_{3\times 1} & \mathbf{0}_{3\times 3} & \mathbf{0}_{3\times 3} & \mathbf{0}_{3\times 1}\\ \mathbf{0}_{1\times 3} & \mathbf{0}_{1\times 3} & \mathbf{0}_{1\times 3} & 1 & \mathbf{0}_{1\times 3} & \mathbf{0}_{1\times 3} & \mathbf{0}_{1\times 1}\end{bmatrix}, \tag{39}$$

which is of full column rank. Thus, system (36) is observable.

2) Unobservable directions of Ω: Based on Theorem 1, the unobservable directions of system (3) lie in the null space of matrix Ω if Ξ is of full rank (see also APPENDIX A). Since the observability of system (36) is proved for two key features ($M=2$), Ω is formed by stacking the derivatives of $\{\beta_{11},\beta_{12},\beta_2,\beta_3,\beta_4,\beta_5,\beta_6\}$ with respect to the state vector $\mathbf{x}$:

$$\Omega = \begin{bmatrix}\mathbf{0}_{3\times 3} & \mathbf{0}_{3\times 3} & \mathbf{0}_{3\times 3} & \mathbf{0}_{3\times 3} & \mathbf{0}_{3\times 3} & \mathbf{I}_3 & \mathbf{0}_{3\times 3}\\ \mathbf{0}_{3\times 3} & \mathbf{0}_{3\times 3} & \mathbf{0}_{3\times 3} & \mathbf{0}_{3\times 3} & \mathbf{0}_{3\times 3} & \mathbf{0}_{3\times 3} & \mathbf{I}_3\\ \mathbf{C}_C\lfloor\mathbf{C}\mathbf{e}_r\rfloor\frac{\partial^I\theta_G}{\partial^I\mathbf{s}_G} & \mathbf{0}_{3\times 3} & \mathbf{0}_{3\times 3} & \lfloor\mathbf{C}_C\mathbf{C}\mathbf{e}_r\rfloor\frac{\partial^C\theta_I}{\partial^C\mathbf{s}_I} & \mathbf{0}_{3\times 3} & \mathbf{0}_{3\times 3} & \mathbf{0}_{3\times 3}\\ \mathbf{0}_{1\times 3} & \mathbf{0}_{1\times 3} & \mathbf{e}_r^{\top} & \mathbf{0}_{1\times 3} & \mathbf{0}_{1\times 3} & \mathbf{0}_{1\times 3} & \mathbf{0}_{1\times 3}\\ \mathbf{0}_{3\times 3} & \mathbf{0}_{3\times 3} & \mathbf{0}_{3\times 3} & \mathbf{I}_3 & \mathbf{0}_{3\times 3} & \mathbf{0}_{3\times 3} & \mathbf{0}_{3\times 3}\\ \mathbf{0}_{3\times 3} & \mathbf{0}_{3\times 3} & \mathbf{0}_{3\times 3} & \mathbf{0}_{3\times 3} & \mathbf{I}_3 & \mathbf{0}_{3\times 3} & \mathbf{0}_{3\times 3}\\ \mathbf{0}_{1\times 3} & \mathbf{e}_r^{\top} & \mathbf{0}_{1\times 3} & \mathbf{0}_{1\times 3} & \mathbf{0}_{1\times 3} & \mathbf{0}_{1\times 3} & \mathbf{0}_{1\times 3}\end{bmatrix}. \tag{40}$$

To derive the full null space of Ω, we need to find a matrix

$$\mathbf{N} = [\mathbf{N}_1^{\top}\ \mathbf{N}_2^{\top}\ \mathbf{N}_3^{\top}\ \mathbf{N}_4^{\top}\ \mathbf{N}_5^{\top}\ \mathbf{N}_6^{\top}\ \mathbf{N}_7^{\top}]^{\top} \neq \mathbf{0}, \tag{41}$$

such that

$$\Omega\mathbf{N} = \mathbf{0}. \tag{42}$$

From (42), we have:

- Multiplying the first, second, fifth, and sixth block rows of Ω with $\mathbf{N}$, we get $\mathbf{N}_4 = \mathbf{N}_5 = \mathbf{N}_6 = \mathbf{N}_7 = \mathbf{0}$.

[3] It is worth mentioning that our observability proof for system (19) is made under the condition that we select at least two key features and the orthogonal velocity of the IMU with respect to the mirror is not zero. However, a proof with relaxed conditions might be feasible by investigating the higher order Lie derivatives.

- Multiplying the third block row of Ω with $\mathbf{N}$, we have $\mathbf{C}_C\lfloor \mathbf{C}\mathbf{e}_r \rfloor \frac{\partial {}^I\theta_G}{\partial {}^I\mathbf{s}_G}\mathbf{N}_1 = \mathbf{0}$, which implies that either $\mathbf{N}_1 = \mathbf{0}$ or $\mathbf{N}_1 = \frac{\partial {}^I\mathbf{s}_G}{\partial {}^I\theta_G}\mathbf{C}\mathbf{e}_r$.
- From the fourth and seventh block rows of $\Omega\mathbf{N} = \mathbf{0}$ we have: $\mathbf{e}_r^\top \mathbf{N}_3 = 0$ and $\mathbf{e}_r^\top \mathbf{N}_2 = 0$. This implies that $\mathbf{N}_2$ and $\mathbf{N}_3$ are spanned by $\{\mathbf{e}_j, \mathbf{e}_d\}$ for $j,d \in \{0,1,2,3\}$, such that $\mathbf{e}_r^\top \mathbf{e}_j = \mathbf{e}_r^\top \mathbf{e}_d = 0$ where $\mathbf{e}_j^\top \mathbf{e}_d = 0$.

By stacking all the combinations of $\mathbf{N}_1, \mathbf{N}_2, \mathbf{N}_3$ in $\mathbf{N}$, we can see that only five columns are linearly independent. That is, the null space of system (3) is spanned by five directions:

$$\mathbf{N} = \begin{bmatrix} \mathbf{0}_{3\times 2} & \mathbf{0}_{3\times 2} & \frac{\partial {}^I\mathbf{s}_G}{\partial {}^I\theta_G}\mathbf{C}\mathbf{e}_r \\ \begin{bmatrix} \mathbf{e}_j & \mathbf{e}_d \end{bmatrix} & \mathbf{0}_{3\times 2} & \mathbf{0}_{3\times 1} \\ \mathbf{0}_{3\times 2} & \begin{bmatrix} \mathbf{e}_j & \mathbf{e}_d \end{bmatrix} & \mathbf{0}_{3\times 1} \\ \mathbf{0}_{3\times 2} & \mathbf{0}_{3\times 2} & \mathbf{0}_{3\times 1} \\ \mathbf{0}_{3\times 2} & \mathbf{0}_{3\times 2} & \mathbf{0}_{3\times 1} \\ \mathbf{0}_{3\times 2} & \mathbf{0}_{3\times 2} & \mathbf{0}_{3\times 1} \\ \mathbf{0}_{3\times 2} & \mathbf{0}_{3\times 2} & \mathbf{0}_{3\times 1} \end{bmatrix}, \tag{43}$$

which implies that the IMU-camera calibration parameters and the 3D positions of the key features with respect to the camera are all observable. Moreover, the unobservable directions correspond to the system's planar translation and velocity orthogonal to $\mathbf{e}_r$ (first and second block columns of $\mathbf{N}$) and rotation around $\mathbf{e}_r$ (third block column of $\mathbf{N}$).

V. Estimation Framework

In this section, we first describe the system process model in the form of an error state model based on the inertial measurements in Section V-A. Then, the measurement model from the camera is presented in Section V-B. Finally, the statistics of the random variables under the constructed nonlinear process model (2) and the nonlinear measurement equation (3) are estimated in an unscented Kalman filter framework (Algorithm 1).

A. Propagation model

We define the inertial navigation system (INS) state vector as:

$$\mathbf{x}^{\text{ins}} = [{}^I\mathbf{q}_G{}^\top \quad {}^G\mathbf{v}_I{}^\top \quad {}^G\mathbf{p}_I{}^\top \quad \mathbf{b}_a^\top \quad \mathbf{b}_g^\top]^\top, \tag{44}$$

where ${}^I\mathbf{q}_G$ is the quaternion that represents the orientation of the global frame $\{G\}$ in the IMU's frame of reference $\{I\}$; $\mathbf{b}_a$ and $\mathbf{b}_g$ are the bias vectors affecting the accelerometer and gyroscope measurements, respectively.

The time evolution of the INS state is described by

$$\begin{aligned} {}^I\dot{\mathbf{q}}_G(t) &= \frac{1}{2}\begin{bmatrix} -\lfloor \omega(t) \rfloor & \omega(t) \\ -\omega(t)^\top & 0 \end{bmatrix} {}^I\mathbf{q}_G(t), \qquad (45)\\ {}^G\dot{\mathbf{v}}_I(t) &= {}^G\mathbf{a}(t) = {}^G\mathbf{g} + \mathbf{C}({}^I\mathbf{q}_G(t))^\top ({}^I\mathbf{a}(t) - \mathbf{b}_a(t)), \\ {}^G\dot{\mathbf{p}}_I(t) &= {}^G\mathbf{v}_I(t), \qquad \dot{\mathbf{b}}_a(t) = \mathbf{n}_{\delta a}, \qquad \dot{\mathbf{b}}_g(t) = \mathbf{n}_{\delta g}, \end{aligned}$$

where $\mathbf{n}_{\delta g}$ and $\mathbf{n}_{\delta a}$ are the accelerometer and gyroscope bias driving white Gaussian noises. The output measurement signals of the gyroscope, ω_m, and accelerometer, $\mathbf{a}_m$, are modeled as:

$$\omega_m(t) = \omega(t) + \mathbf{b}_g(t) + \mathbf{n}_g(t) \tag{46}$$

$$\mathbf{a}_m(t) = \mathbf{C}({}^C\mathbf{q}_G(t))({}^G\mathbf{a} - {}^G\mathbf{g}) + \mathbf{b}_a(t) + \mathbf{n}_a(t). \tag{47}$$

For the state estimation, we use the system discrete-time error state space model, which is derived from (45) based on the standard additive error definition for the position, velocity, and biases ($\delta x \simeq x - \hat{x}$), and quaternion error for the rotational euler angles θ ($\delta\mathbf{q} \simeq [1 \quad \frac{\delta\theta}{2}^\top]^\top$). Then the concatenated INS error state vector is

$$\delta\mathbf{x}^{\text{ins}} = [\delta {}^I\theta_G^\top \quad \delta {}^G\mathbf{v}_I{}^\top \quad \delta {}^G\mathbf{p}_I^\top \quad \delta\mathbf{b}_a^\top \quad \delta\mathbf{b}_g^\top]^\top, \tag{48}$$

and the total error state vector from (1) is

$$\delta\mathbf{x} = [\delta\mathbf{x}^{\text{ins}\top} \quad \delta {}^C\theta_I^\top \quad \delta {}^I\mathbf{p}_C^\top \quad \delta {}^C\mathbf{p}_{f_1}{}^\top \quad \cdots \quad \delta {}^C\mathbf{p}_{f_M}{}^\top]^\top. \tag{49}$$

During a short period of time δt, we approximate the nonlinear INS propagation model (2) in the form of a discrete-time linear state-space model

$$\delta\mathbf{x}_{k+1} = \mathbf{F}_k\delta\mathbf{x}_k + \mathbf{G}_k\mathbf{n}_k \in \mathbb{R}^{15+6+3M}, \tag{50}$$

where $\mathbf{F}_k$ and $\mathbf{G}_k$ are known as discrete time state and system noise propagation matrices, respectively:

$$\mathbf{F}_k = \begin{bmatrix} \bar{\mathbf{F}}_k & \mathbf{0}_{15\times(6+3M)} \\ \mathbf{0}_{(6+3M)\times 15} & \mathbf{I}_{(6+3M)\times(6+3M)} \end{bmatrix}, \tag{51}$$

where

$$\bar{\mathbf{F}}_k = \begin{bmatrix} \mathbf{I}_3 & \mathbf{0}_{3\times 3} & \mathbf{0}_{3\times 3} & \mathbf{0}_{3\times 3} & -dt\mathbf{C}({}^C\hat{\mathbf{q}}_G) \\ dt\lfloor \mathbf{C}({}^C\hat{\mathbf{q}}_G)\hat{\mathbf{a}} \rfloor & \mathbf{I}_3 & \mathbf{0}_{3\times 3} & dt\mathbf{C}({}^C\hat{\mathbf{q}}_G) & \mathbf{0}_{3\times 3} \\ \mathbf{0}_{3\times 3} & dt\mathbf{I}_3 & \mathbf{I}_3 & \mathbf{0}_{3\times 3} & \mathbf{0}_{3\times 3} \\ \mathbf{0}_{3\times 3} & \mathbf{0}_{3\times 3} & \mathbf{0}_{3\times 3} & \mathbf{I}_{3\times 3} & \mathbf{0}_{3\times 3} \\ \mathbf{0}_{3\times 3} & \mathbf{0}_{3\times 3} & \mathbf{0}_3 & \mathbf{0}_{3\times 3} & \mathbf{I}_3 \end{bmatrix},$$

and

$$\mathbf{G}_k = \begin{bmatrix} \mathbf{0}_{3\times 3} & -dt\mathbf{C}({}^C\hat{\mathbf{q}}_G) & \mathbf{0}_{3\times 3} & \mathbf{0}_{3\times 3} \\ dt\mathbf{C}({}^C\hat{\mathbf{q}}_G) & \mathbf{0}_{3\times 3} & \mathbf{0}_{3\times 3} & \mathbf{0}_{3\times 3} \\ \mathbf{0}_{3\times 3} & \mathbf{0}_{3\times 3} & \mathbf{0}_{3\times 3} & \mathbf{0}_{3\times 3} \\ \mathbf{0}_{3\times 3} & \mathbf{0}_{3\times 3} & dt\mathbf{I}_3 & \mathbf{0}_{3\times 3} \\ \mathbf{0}_{3\times 3} & \mathbf{0}_{3\times 3} & \mathbf{0}_{3\times 3} & dt\mathbf{I}_3 \\ \mathbf{0}_{6\times 3} & \mathbf{0}_{6\times 3} & \mathbf{0}_{6\times 3} & \mathbf{0}_{6\times 3} \\ \mathbf{0}_{3\times 3} & \mathbf{0}_{3\times 3} & \mathbf{0}_{3\times 3} & \mathbf{0}_{3\times 3} \\ \vdots & \vdots & \vdots & \vdots \\ \mathbf{0}_{3\times 3} & \mathbf{0}_{3\times 3} & \mathbf{0}_{3\times 3} & \mathbf{0}_{3\times 3} \end{bmatrix}. \tag{52}$$

$\mathbf{n}_k = [\mathbf{n}_a^\top \quad \mathbf{n}_g^\top \quad \mathbf{n}_{\delta a}^\top \quad \mathbf{n}_{\delta g}^\top]^\top$ is the process noise (assumed to be stationary) with the corresponding diagonal covariance matrix $\mathbf{Q} \in \mathbb{R}^{12\times 12}$, $\mathbf{C}({}^C\hat{\mathbf{q}}_G)$ is the estimated rotation matrix, and $\hat{\mathbf{a}} = \mathbf{a}_m - \hat{\mathbf{b}}_a$.

B. Camera measurement

When the camera along with the IMU is moving in front of a planar mirror, the body frame angular velocity and specific force are measured by the IMU. Meanwhile, the camera records images of the virtual features. The camera measurement of the reflected feature point (following (3)) can be represented as

$$\tilde{\mathbf{z}}_k = \begin{bmatrix} u_k \\ v_k \end{bmatrix} + \mathbf{v}_k = \begin{bmatrix} 1 & 0 & 0 \\ 0 & 1 & 0 \end{bmatrix} \frac{1}{\mathbf{e}_3^\top {}^C\acute{\mathbf{p}}_{f_k}} {}^C\acute{\mathbf{p}}_{f_k} + \mathbf{v}_k, \tag{53}$$

where $\mathbf{v}_k$ is the feature-measurement noise with covariance matrix $\mathbf{R}_k = \sigma_v^2\mathbf{I}_2$ Hence, the measurement model of the system (53) for M observed reflected feature points is

$$\bar{\mathbf{z}} = \bar{\mathbf{h}}(\mathbf{x}) + \bar{\mathbf{v}} \in \mathbb{R}^{2M}, \tag{54}$$

assuming the measurement noise from each projection of the reflected features to be mutually uncorrelated, the covariance matrix of $\bar{\mathbf{v}}$, $\bar{\mathbf{R}}^{2M\times 2M}$, will be a block-diagonal.

Finally, the joint state-space model of the system can be constructed from the error propagation (50) along with the measurement equation (54). An overview of the estimation algorithm is given in Algorithm 1. In this algorithm, χ_l is the l-th column of the sigma-points matrix χ, N is the length of the state vector. $\bar{\mathbf{R}}_m$ is the measurement noise covariance matrix at m-th step, $\mathbf{G}$ is the system noise propagation matrix and $\mathbf{Q}$ is the process noise covariance matrix. The weights of the sigma-points w_l^c, w_l^m are set to $\frac{1}{2(N+1)}$ for $l=1,\cdots,2N$, and for $l=0$ we have $w_0^c=\frac{\lambda}{N+\lambda}+(1-\alpha^2+\beta)$, $w_0^m=\frac{\lambda}{N+\lambda}$. The scaling parameter $\lambda=\alpha^2(N+\kappa)-N$, and $\eta=\sqrt{N+\lambda}$ are set using $\alpha=0.1$, $\beta=2$, and $\kappa=0$, [19].

Algorithm 1

Initialize $\hat{\mathbf{x}}_0^-$ and $\mathbf{P}_0^-$
for $n=0$:end **do**
  INS equation update
  if the measurement from the camera is ready **then**
    $\bar{\mathbf{z}}_n=[\bar{\mathbf{z}}_1^\top,\bar{\mathbf{z}}_2^\top,\cdots,\bar{\mathbf{z}}_M^\top]^\top$ $\%from$ (53)
    $\bar{\mathbf{R}}_n=\mathrm{diag}(\mathbf{R}_k)\,\%\,k=1,\cdots,M$
    $\xi_{l,n}^-=\mathbf{h}_n(\chi_{l,n}^-)$
    $\hat{\bar{\mathbf{z}}}_n^-=\sum_{l=0}^{2N}w_l^m\xi_{l,n}^-$
    $\%Measurement\ update$
    $\mathbf{R}_{e,n}=\sum_{l=0}^{2N}w_l^m(\xi_{l,n}^--\hat{\bar{\mathbf{z}}}_n^-)(\xi_{l,n}^--\hat{\bar{\mathbf{z}}}_n^-)^*+\bar{\mathbf{R}}_n$
    $\mathbf{R}_{x,e,n}=\sum_{l=0}^{2N}w_l^m(\chi_{l,n}^--\hat{\mathbf{x}}_n^-)(\xi_{l,n}^--\hat{\bar{\mathbf{z}}}_n^-)^*$
    $\mathbf{K}_n=\mathbf{R}_{x,e,n}\mathbf{R}_{e,n}^{-1}$
    $\hat{\mathbf{x}}_n=\hat{\mathbf{x}}_n^-+\mathbf{K}_n(\bar{\mathbf{z}}_n-\bar{\mathbf{z}}_n^-)$
    $\mathbf{P}_n=\mathbf{P}_n^--\mathbf{K}_n\mathbf{R}_{e,n}\mathbf{K}_n^*$
    $\mathbf{s}_n=\hat{\mathbf{x}}_n$
    $\mathbf{S}_n=\mathbf{P}_n$
  else
    $\mathbf{s}_n=\hat{\mathbf{x}}_n^-$
    $\mathbf{S}_n=\mathbf{P}_n^-$
  end if
  $\%Sigma-Point\ generation$
  $\chi_n=[\mathbf{s}_n\quad \mathbf{s}_n+\eta\sqrt{\mathbf{S}_n}\quad \mathbf{s}_n-\eta\sqrt{\mathbf{S}_n}]$
  $\chi_n^-=f_k(\chi_{l,n})$
  $\%Time\ update$
  $\hat{\mathbf{x}}_{n+1}^-=\sum_{l=0}^{2N}w_l^m\chi_{l,n+1}^-$
  $\mathbf{P}_{n+1}^-=\sum_{l=0}^{2N}w_l^c(\chi_{l,n+1}^--\hat{\mathbf{x}}_{n+1}^-)(\chi_{l,n+1}^--\hat{\mathbf{x}}_{n+1}^-)^*+\mathbf{GQG}^*$
end for

VI. Performance Evaluation

The proposed calibration approach has been extensively evaluated using both simulations and experiments. Some of the results are given in the following.

A. Simulation results

Fig. 4 shows a sample trajectory used for performance evaluation of the estimator within a period of 120 s. The sampling rate of the IMU is 100 Hz. The camera sampling rate is 10 Hz and its intrinsic parameters are set to $k_u=k_v=833$, $p_u=2$, $p_v=8$, and $s=3$ [26]. The IMU-camera relative translation is ${}^I\mathbf{p}_C=[5\ -5\ 10]^\top$ cm and the relative rotation angles are set to ${}^C\theta_I=[-90^\circ\ 0^\circ\ -90^\circ]^\top$. The projections of the key

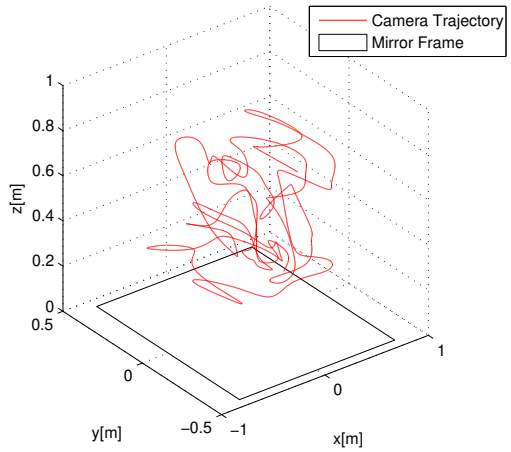

Fig. 4: Simulated IMU-camera trajectory over a planar mirror, for 120 s. In this scenario, the normal of the mirror is aligned with the gravity along the z axis (taken from [17]).

features' reflections in the image plane are corrupted with additive zero-mean Gaussian noise with a standard deviation of $\sigma_v=2$ pixels.

To examine the key finding of our observability analysis, we performed 100 Monte Carlo simulations to get estimates of the errors in the state variables (1). Fig. 5(a)–Fig. 5(c) show the estimated mean errors along with the 3σ bounds for the IMU-camera relative rotation, translation, position and attitude. The results are achieved using only two key features whose reflections were tracked in the images over time. The 3σ values are computed from the corresponding diagonal elements of the filter's error covariance matrix that provides a representation of its estimate uncertainty. As we expected, the estimated errors remain bounded for the observable states (IMU-camera relative rotation and translation, IMU orthogonal distance to the mirror, IMU roll and pitch, and the 3D positions of the key features with respect to the camera). Also, Fig. 5(c) and Fig. 5(d) show that the uncertainties of the errors are increasing along the unobservable states, which is in line with our theoretical results.

Table I summarizes the final estimated mean values and the standard deviations of the errors (σ) for IMU-camera 6-DoF, translations and rotations, where different numbers of key features (KF) are used in each of the experiments. Simulation results show that the proposed estimation method is able to reach subcentimeter and subdegree accuracy for the IMU-camera rotation and translation. As can be noticed, we can achieve a good level of accuracy using only two key features, and the estimation uncertainties decrease only marginally by observing more key features. The proposed estimation algorithm is quite modest in complexity because of the involved basic algebraic functions. Noticeably, from the filter computational point of view, the length of the state vector in our method is fixed to $15+6+3M$ and the computational complexity is mainly determined (excluding feature detection and matching) by matrix inversions in the Kalman filtering. Code optimization was not a part of the study and a Matlab

implementation running on a standard laptop was used for our implementation. The processing time ratio increasing the number of features is given by 1:1.2:2.4 for two, three and six features, respectively.

TABLE I: Initial, final, and error statistics of the IMU-camera calibration parameters, using the simulation data.

	$\mathbf{p}^b_{c,x} \pm \sigma$[cm]	$\mathbf{p}^b_{c,y} \pm \sigma$ [cm]	$\mathbf{p}^b_{c,z} \pm \sigma$[cm]
Initial	0 ± 1	0 ± 1	0 ± 1
Final (2 KF)	4.2 ± 0.72	-5.56 ± 0.22	10.72 ± 0.4
Final (3 KF)	5.1 ± 0.6	-5.1 ± 0.16	10.68 ± 0.32
Final (6 KF)	5.52 ± 0.5	-5.23 ± 0.15	10.3 ± 0.29
	$\varphi_\phi \pm \sigma[^\circ]$	$\varphi_\theta \pm \sigma[^\circ]$	$\varphi_\psi \pm \sigma[^\circ]$
Initial	-70 ± 2	10 ± 2	-100 ± 2
Final (2 KF)	-89.99 ± 0.02	0 ± 0.2	-89.99 ± 0.07
Final (3 KF)	-90 ± 0.01	0 ± 0.02	-90 ± 0.06
Final (6 KF)	-90 ± 0.01	0 ± 0.01	-90 ± 0.06

B. Experimental results

We studied the performance of the proposed calibration method using experimental data. To concentrate our experiments on validating our theoretical analysis, we used a checkerboard pattern attached to the IMU-camera where its corners were selected as the candidate's key features. Hence, the feature detection and tracking can be performed with high accuracy, which in turn helped us to examine our calibration method without being affected by the possible errors from the feature detection and tracking. For the feature detection, Harris corner detection was applied to the images, then nearest-neighbor-matching was used for tracking the position of the virtual features. To initialize the IMU attitude, we used the gravitational force during the first samples in which the system was stationary in front of the planar mirror [27]. The initial values of the IMU-camera calibration parameters were set using manual measurements on the hardware.

To better quantify the estimation uncertainty, the 3σ bounds of the error for some of the estimated parameters are plotted. Fig. 6(a) and Fig. 6(b) depict the 3σ bounds of the error for the IMU-camera calibration parameters, where the IMU-camera was moved for a period of 140 s in front of the mirror. Moreover, we have plotted the 3σ bounds for the errors in the IMU position in Fig. 6(c), which gives bounded uncertainties for the IMU orthogonal translation relative to the mirror. As can be noticed, we observe similar behavior for the estimated error between the simulation data and experiments (increasing uncertainty for the unobservable modes and bounded error for the observable modes).

Moreover, Table II reports the final estimated values and the standard deviation of the error (σ) for IMU-camera 6-DoF's translation and rotation, where different numbers of key features are used in the estimation process.

VII. Conclusion

We have proposed an IMU-camera calibration method for estimating the 6-DoF transformation between the IMU-camera rig. In this visual inertial navigation system, the visual corrections are provided by tracking a set of key features' reflections in a planar mirror on the image planes. The key features are positioned at arbitrary unknown locations on the sensors's body, such that their reflections can be observed by the camera. We have studied the observability properties of the calibration parameters for the system when navigating in front of a planar mirror. Through the observability analysis, we have proved that the calibration parameters and the 3D positions of the key features with respect to the camera are observable using only two key features. Moreover, for the analysed nonlinear system, we proposed an estimation approach using the unscented Kalman filter. Finally, the findings of our observability analysis and the proposed estimation approach were evaluated both in simulations and using experimental data. The flexibility and simplicity in addition to the achieved results indicate that the proposed method can conveniently be used in smartphones and off-the-shelf IMU-camera devices, without having access to a calibration target.

TABLE II: Initial, final, and error statistics for the IMU-camera calibration parameters.

	$\mathbf{p}^b_{c,x} \pm \sigma$[cm]	$\mathbf{p}^b_{c,y} \pm \sigma$ [cm]	$\mathbf{p}^b_{c,z} \pm \sigma$[cm]
Initial	0 ± 1	0 ± 1	0 ± 1
Final (2 KF)	-2.7 ± 0.15	-0.56 ± 0.15	1.6 ± 0.16
Final (3 KF)	-2.77 ± 0.15	-0.81 ± 0.15	1.93 ± 0.15
Final (6 KF)	-2.65 ± 0.13	-1.21 ± 0.13	2.57 ± 0.13
	$\varphi_\phi \pm \sigma[^\circ]$	$\varphi_\theta \pm \sigma[^\circ]$	$\varphi_\psi \pm \sigma[^\circ]$
Initial	-85 ± 5	6 ± 5	80 ± 5
Final (2 KF)	-88.9 ± 0.23	0.58 ± 0.23	88.25 ± 0.21
Final (3 KF)	-89.1 ± 0.22	0.54 ± 0.22	88.42 ± 0.20
Final (6 KF)	-89.1 ± 0.19	0.55 ± 0.19	88.44 ± 0.18

References

[1] P. Händel, "Discounted least-squares gearshift detection using accelerometer data," *IEEE Transactions on Instrumentation and Measurement*, vol. 58, pp. 3953–3958, Dec. 2009.

[2] P. Szemes, H. Hashimoto, and P. Korondi, "Pedestrian-behavior-based mobile agent control in intelligent space," *IEEE Transactions on Instrumentation and Measurement*, vol. 54, pp. 2250–2257, Dec. 2005.

[3] G. Panahandeh, N. Mohammadiha, A. Leijon, and P. Händel, "Continuous hidden markov model for pedestrian activity classification and gait analysis," *IEEE Transactions on Instrumentation and Measurement*, vol. 62, no. 5, pp. 1073–1083, 2013.

[4] P. Lang, A. Kusej, A. Pinz, and G. Brasseur, "Inertial tracking for mobile augmented reality," in *Proc. of the 19th IEEE Instrumentation and Measurement Technology Conference, IMTC*, vol. 2, pp. 1583–1587, 2002.

[5] H. Koch, A. Konig, A. Weigl-Seitz, K. Kleinmann, and J. Suchy, "Multisensor contour following with vision, force, and acceleration sensors for an industrial robot," *IEEE Transactions on Instrumentation and Measurement*, vol. 62, no. 2, pp. 268–280, 2013.

[6] Y. Tian, W. Hamel, and J. Tan, "Accurate human navigation using wearable monocular visual and inertial sensors," *IEEE Transactions on Instrumentation and Measurement*, no. 99, 2013.

[7] H. Bacakoglu and M. Kamel, "A three-step camera calibration method," *IEEE Transactions on Instrumentation and Measurement*, vol. 46, no. 5, pp. 1165–1172, 1997.

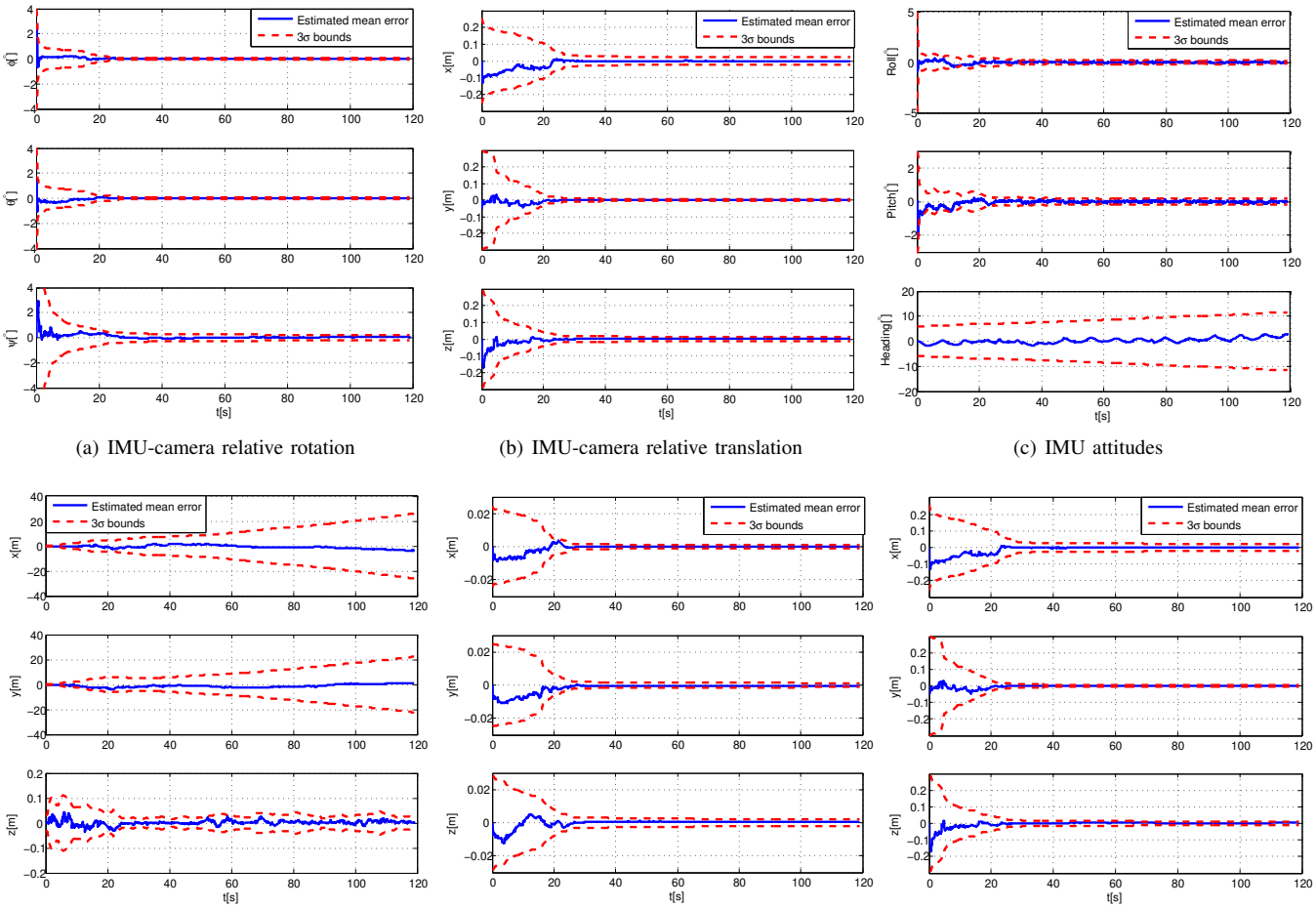

(a) IMU-camera relative rotation (b) IMU-camera relative translation (c) IMU attitudes

(d) IMU positions (e) 3D position of the first KF (f) 3D position of the second KF

Fig. 5: Estimated error and the 3σ bounds for (a) the IMU-camera relative rotation and (b) translations, (c) IMU attitude and (d) position, and (e)–(f) two key features. The results are achieved using the simulation data where the ground truths are available.

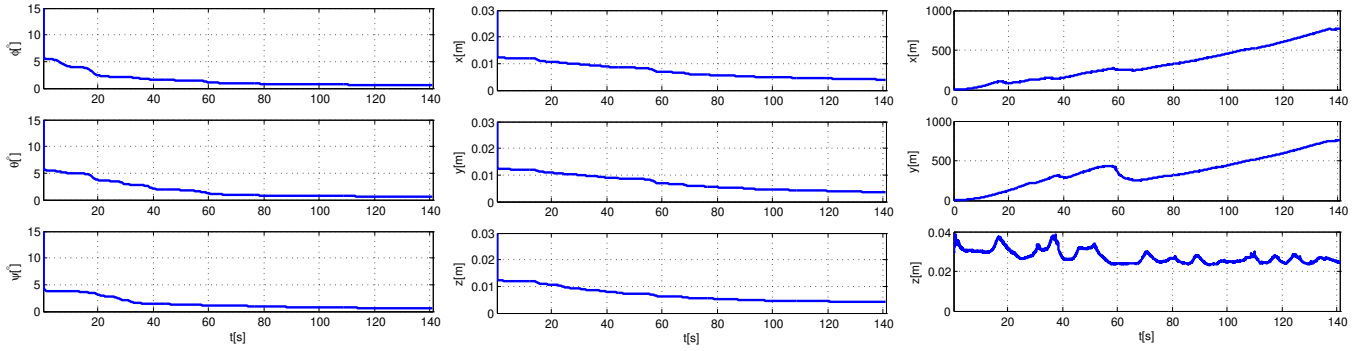

(a) IMU-camera relative rotation (b) IMU-camera relative translation (c) IMU position

Fig. 6: The estimated 3σ bounds for the error in (a) the IMU-camera relative rotation, (b) translation, and (c) IMU position, using the experimental data.

[8] J. Galilea, J.-M. Lavest, C. Vazquez, A. Gardel Vicente, and I. Bravo Munoz, "Calibration of a high-accuracy 3-d coordinate measurement sensor based on laser beam and CMOS camera," *IEEE Transactions on Instrumentation and Measurement*, vol. 58, no. 9, pp. 3341–3346, 2009.

[9] J. Bekkeng, "Calibration of a novel mems inertial reference unit," *IEEE Transactions on Instrumentation and Measurement*, vol. 58, no. 6, pp. 1967–1974, 2009.

[10] S. Vidas, R. Lakemond, S. Denman, C. Fookes, S. Sridharan, and T. Wark, "A mask-based approach for the geometric calibration of thermal-infrared cameras," *IEEE Transactions on Instrumentation and Measurement*, vol. 61, no. 6, pp. 1625–1635, 2012.

[11] J. Li, J. Fang, and M. Du, "Error analysis and gyro-bias calibration of analytic coarse alignment for airborne pos," *IEEE Transactions on Instrumentation and Measurement*, vol. 61, no. 11, pp. 3058–3064, 2012.

[12] J. Lobo and J. Dias, "Vision and inertial sensor cooperation using gravity as a vertical reference," *IEEE Trans. Pattern Anal. Mach. Intell.*, vol. 25, no. 12, pp. 1597–1608, 2003.

[13] E. S. Jones and S. Soatto, "Visual-inertial navigation, mapping and localization: A scalable real-time causal approach," *Int. Journal of Robotics Research*, vol. 30, no. 4, pp. 407–430, 2011.

[14] F. M. Mirzaei and S. I. Roumeliotis, "A Kalman filter-based algorithm for IMU-camera calibration: Observability analysis and performance evaluation," *IEEE Trans. on Robotics*, vol. 24, no. 5, pp. 1143–1156, 2008.

[15] J. Hol, T. Schön, and F. Gustafsson, "Relative pose calibration of a spherical camera and an IMU," in *IEEE/ACM Int. Symposium on Mixed and Augmented Reality, (ISMAR), Cambridge, UK*, pp. 21–24, Sep. 15-18, 2008.

[16] J. Kelly and G. S. Sukhatme, "Visual-inertial sensor fusion: Localization, mapping and sensor-to-sensor self-calibration," *Int. Journal of Robotics Research*, vol. 30, no. 1, pp. 56–79, 2011.

[17] G. Panahandeh and M. Jansson, "IMU-camera self-calibration using planar mirror reflection," in *Proc. IEEE Int. Conf. on Indoor Positioning and Indoor Navigation (IPIN), Guimares, Portugal*, pp. 1–7, Sep. 21-23, 2011.

[18] C. X. Guo and S. I. Roumeliotis, "IMU-RGBD camera extrinsic calibration: Observability analysis and consistency improvement," in *Proc. IEEE Int. Conf. on Robotics and Automation (ICRA), Karlsruhe, Germany*, pp. 2920–2927, May 6-10, 2013.

[19] S. J. Julier and J. K. Uhlmann, "A new extension of the Kalman filter to nonlinear systems," in *Proc. of Signal Processing, Sensor fusion, and Target Recognition*, vol. 4, pp. 182–193, Apr. 1997.

[20] G. Panahandeh, D. Zachariah, and M. Jansson, "Mirror based IMU-camera and internal camera calibration," in *Proc. IEEE Int. Conf. on Robot, Vision and Signal Processing (RVSP), Kaohsiung, Taiwan*, pp. 199–203, Nov. 21-23, 2011.

[21] J. A. Hesch, A. I. Mourikis, and S. I. Roumeliotis, "Mirror-based extrinsic camera calibration," in *Int. Workshop on the Algorithmic Foundations of Robotics, Mexico*, Dec. 2008.

[22] J. Gluckman and S. Nayar, "Planar catadioptric stereo: geometry and calibration," in *Proc. of Computer Vision and Pattern Recognition. IEEE Computer Society Conf.*, vol. 1, p. 2, 1999.

[23] J. Gluckman and S. K. Nayar, "Catadioptric stereo using planar mirrors," *Int. J. Comput. Vision*, vol. 44, pp. 65–79, Aug. 2001.

[24] M. D. Shuster, "A survey of attitude representations," *Astronautical Sciences*, vol. 41, no. 4, pp. 439–517, 1993.

[25] R. Hermann and A. Krener, "Nonlinear controllability and observability," *IEEE Trans. on Automatic Control*, vol. 22, no. 4, pp. 728–740, 1977.

[26] R. I. Hartley and A. Zisserman, *Multiple View Geometry in Computer Vision*. Cambridge University Press, ISBN: 0521623049, 2000.

[27] G. Panahandeh, I. Skog, and M. Jansson, "Calibration of the accelerometer triad of an inertial measurement unit, maximum likelihood estimation and Cramer-Rao bound," in *IEEE Int. Conf. on Indoor Positioning and Indoor Navigation (IPIN), Zurich, Switzerland*, pp. 1–6, Sep. 15-17, 2010.

APPENDIX A

Here, we compute only those Lie derivatives of $\bar{\mathbf{h}}_1$ and $\bar{\mathbf{h}}_2$ whose derivatives are used to prove that Ξ is of full column rank.

- The zeroth order Lie derivative of a function is the function itself, i.e.,

$$\mathfrak{L}^0\bar{\mathbf{h}}_1 = \mathbf{T}_1(\beta_{11} - 2\beta_2\beta_2^\top\beta_{11} - 2\beta_2\beta_3 - 2\beta_2\beta_2^\top\mathbf{C}(\beta_4)\beta_5), \tag{55}$$

$$\mathfrak{L}^0\bar{\mathbf{h}}_2 = \mathbf{T}_2(\beta_{12} - 2\beta_2\beta_2^\top\beta_{12} - 2\beta_2\beta_3 - 2\beta_2\beta_2^\top\mathbf{C}(\beta_4)\beta_5). \tag{56}$$

Then the gradients (the spans) of the zeroth order Lie derivatives are

$$\nabla\mathfrak{L}^0\bar{\mathbf{h}}_1 = \mathbf{T}_1\begin{bmatrix}\mathbf{I}_3 - 2\beta_2\beta_2^\top & \mathbf{0}_{3\times3} & \Pi_{21} & -2\beta_2 & -2\beta_2\beta_2^\top\frac{\partial\mathbf{C}(\beta_4)\beta_5}{\partial\beta_4} & -2\beta_2\beta_2^\top\mathbf{C}(\beta_4) & \mathbf{0}_{3\times1}\end{bmatrix}, \tag{57}$$

$$\nabla\mathfrak{L}^0\bar{\mathbf{h}}_2 = \mathbf{T}_2\begin{bmatrix}\mathbf{0}_{3\times3} & \mathbf{I}_3 - 2\beta_2\beta_2^\top & \Pi_{22} & -2\beta_2 & -2\beta_2\beta_2^\top\frac{\partial\mathbf{C}(\beta_4)\beta_5}{\partial\beta_4} & -2\beta_2\beta_2^\top\mathbf{C}(\beta_4) & \mathbf{0}_{3\times1}\end{bmatrix}, \tag{58}$$

where

$$\Pi_{2k} = -2\beta_2^\top\beta_{1k}\mathbf{I}_3 - 2\beta_2\beta_{1k}^\top - 2\beta_3\mathbf{I}_3 - 2\beta_2^\top\mathbf{C}(\beta_4)\beta_5\mathbf{I}_3 - 2\beta_2\beta_5^\top\mathbf{C}(\beta_4)^\top. \tag{59}$$

- The first order Lie derivatives of $\bar{\mathbf{h}}_k$ with respect to $\mathbf{g}_0$, and $\mathbf{g}_{1i}$ are computed respectively as:

$$\mathfrak{L}^1_{\mathbf{g}_0}\bar{\mathbf{h}}_1 = \nabla\mathfrak{L}^0\bar{\mathbf{h}}_1\mathbf{g}_0 = -2\beta_2\beta_6, \tag{60}$$

$$\mathfrak{L}^1_{\mathbf{g}_{1i}}\bar{\mathbf{h}}_1 = \nabla\mathfrak{L}^0\bar{\mathbf{h}}_1\mathbf{g}_{1i} = \Pi_{21}\lfloor\beta_2\rfloor\mathbf{C}(\beta_4)\mathbf{e}_i, \tag{61}$$

$$\mathfrak{L}^1_{\mathbf{g}_0}\bar{\mathbf{h}}_2 = \nabla\mathfrak{L}^0\bar{\mathbf{h}}_2\mathbf{g}_0 = -2\beta_2\beta_6, \tag{62}$$

$$\mathfrak{L}^1_{\mathbf{g}_{1i}}\bar{\mathbf{h}}_2 = \nabla\mathfrak{L}^0\bar{\mathbf{h}}_2\mathbf{g}_{1i} = \Pi_{22}\lfloor\beta_2\rfloor\mathbf{C}(\beta_4)\mathbf{e}_i, \tag{63}$$

and the gradients that correspond with them are given by

$$\nabla\mathfrak{L}^1_{\mathbf{g}_0}\bar{\mathbf{h}}_1 = \frac{\partial\mathfrak{L}^1_{\mathbf{g}_0}\bar{\mathbf{h}}_1}{\partial\beta} = \mathbf{T}_1\begin{bmatrix}\mathbf{0}_{3\times3} & \mathbf{0}_{3\times3} & -2\beta_6\mathbf{I}_3 & \mathbf{0}_{3\times3} & \mathbf{0}_{3\times3} & \mathbf{0}_{3\times3} & -2\beta_2\end{bmatrix}, \tag{64}$$

$$\nabla\mathfrak{L}^1_{\mathbf{g}_{1i}}\bar{\mathbf{h}}_1 = \frac{\partial\mathfrak{L}^1_{\mathbf{g}_{1i}}\bar{\mathbf{h}}_1}{\partial\beta} = \mathbf{T}_1\begin{bmatrix}\bar{\Pi}_{11i} & \mathbf{0}_{3\times3} & \bar{\Pi}_{21i} & \bar{\Pi}_{31i} & \bar{\Pi}_{41i} & \bar{\Pi}_{51i} & \mathbf{0}_{3\times1}\end{bmatrix}, \tag{65}$$

$$\nabla\mathfrak{L}^1_{\mathbf{g}_0}\bar{\mathbf{h}}_2 = \frac{\partial\mathfrak{L}^1_{\mathbf{g}_0}\bar{\mathbf{h}}_2}{\partial\beta} = \mathbf{T}_2\begin{bmatrix}\mathbf{0}_{3\times3} & \mathbf{0}_{3\times3} & -2\beta_6\mathbf{I}_3 & \mathbf{0}_{3\times3} & \mathbf{0}_{3\times3} & \mathbf{0}_{3\times3} & -2\beta_2\end{bmatrix}, \tag{66}$$

$$\nabla\mathfrak{L}^1_{\mathbf{g}_{1i}}\bar{\mathbf{h}}_2 = \frac{\partial\mathfrak{L}^1_{\mathbf{g}_{1i}}\bar{\mathbf{h}}_2}{\partial\beta} = \mathbf{T}_2\begin{bmatrix}\mathbf{0}_{3\times3} & \bar{\Pi}_{12i} & \bar{\Pi}_{22i} & \bar{\Pi}_{32i} & \bar{\Pi}_{42i} & \bar{\Pi}_{52i} & \mathbf{0}_{3\times1}\end{bmatrix}, \tag{67}$$

where

$$\bar{\Pi}_{1ki} = -2\lfloor\beta_2\rfloor\mathbf{C}(\beta_4)\mathbf{e}_i\beta_2^\top - 2\beta_2(\lfloor\beta_2\rfloor\mathbf{C}(\beta_4)\mathbf{e}_i)^\top, \tag{68}$$

$$\bar{\Pi}_{2ki} = -\Pi_{2k}\lfloor\mathbf{C}(\beta_4)\mathbf{e}_i\rfloor - 2\lfloor\beta_2\rfloor\mathbf{C}(\beta_4)\mathbf{e}_i\beta_{1k}^\top - 2\beta_{1k}^\top\lfloor\beta_2\rfloor\mathbf{C}(\beta_4)\mathbf{e}_i\mathbf{I}_3 - 2\lfloor\beta_2\rfloor\mathbf{C}(\beta_4)\mathbf{e}_i\beta_5^\top\mathbf{C}(\beta_4)^\top - 2\beta_5^\top\mathbf{C}(\beta_4)^\top\lfloor\beta_2\rfloor\mathbf{C}(\beta_4)\mathbf{e}_i\mathbf{I}_3, \tag{69}$$

$$\bar{\Pi}_{3ki} = -2\lfloor\beta_2\rfloor\mathbf{C}(\beta_4)\mathbf{e}_i, \tag{70}$$

$$\bar{\Pi}_{5ki} = -2\lfloor\beta_2\rfloor\mathbf{C}(\beta_4)\mathbf{e}_i\beta_2^\top\mathbf{C}(\beta_4) - 2\beta_2(\lfloor\beta_2\rfloor\mathbf{C}(\beta_4)\mathbf{e}_i)^\top\mathbf{C}(\beta_4). \tag{71}$$

- The second order Lie derivatives and their gradients that correspond with them are as follows:

$$\mathfrak{L}^2_{\mathbf{g}_0\mathbf{g}_{1i}}\bar{\mathbf{h}}_1 = \nabla\mathfrak{L}^1_{\mathbf{g}_0}\bar{\mathbf{h}}_1\mathbf{g}_{1i} = -2\beta_6\lfloor\beta_2\rfloor\mathbf{C}(\beta_4)\mathbf{e}_i, \tag{72}$$

$$\mathfrak{L}^2_{\mathbf{g}_0\mathbf{g}_{2i}}\bar{\mathbf{h}}_1 = \nabla\mathfrak{L}^1_{\mathbf{g}_0}\bar{\mathbf{h}}_1\mathbf{g}_{2i} = -2\beta_2\beta_2^\top\mathbf{C}(\beta_4)\mathbf{e}_i, \tag{73}$$

$$\mathfrak{L}^2_{\mathbf{g}_{1i}\mathbf{g}_{1j}}\bar{\mathbf{h}}_1 = \nabla\mathfrak{L}^1_{\mathbf{g}_{1i}}\bar{\mathbf{h}}_1\mathbf{g}_{1j} = \bar{\Pi}_{21i}\lfloor\beta_2\rfloor\mathbf{C}(\beta_4)\mathbf{e}_j, \tag{74}$$

$$\nabla\mathfrak{L}^2_{\mathbf{g}_0\mathbf{g}_{1i}}\bar{\mathbf{h}}_1 = \frac{\partial\mathfrak{L}^2_{\mathbf{g}_0\mathbf{g}_{1i}}\bar{\mathbf{h}}_1}{\partial\beta} = \mathbf{T}_1\begin{bmatrix}\mathbf{0}_{3\times3} & \mathbf{0}_{3\times3} & 2\beta_6\lfloor\mathbf{C}(\beta_4)\mathbf{e}_i\rfloor & \mathbf{0}_{3\times3} & -2\beta_6\lfloor\beta_2\rfloor\frac{\partial\mathbf{C}(\beta_4)\mathbf{e}_i}{\partial\beta_4} & \mathbf{0}_{3\times3} & -2\lfloor\beta_2\rfloor\mathbf{C}(\beta_4)\mathbf{e}_i\end{bmatrix}, \tag{75}$$

$$\nabla\mathfrak{L}^2_{\mathbf{g}_0\mathbf{g}_{2i}}\bar{\mathbf{h}}_1 = \frac{\partial\mathfrak{L}^2_{\mathbf{g}_0\mathbf{g}_{2i}}\bar{\mathbf{h}}_1}{\partial\beta} = \mathbf{T}_1\begin{bmatrix}\mathbf{0}_{3\times3} & \mathbf{0}_{3\times3} & -2\beta_2^\top\mathbf{C}(\beta_4)\mathbf{e}_i\mathbf{I}_3 - 2\beta_2\mathbf{e}_i^\top\mathbf{C}(\beta_4)^\top & \mathbf{0}_{3\times3} & -2\beta_2\beta_2^\top\frac{\partial\mathbf{C}(\beta_4)\mathbf{e}_i}{\partial\beta_4} & \mathbf{0}_{3\times3} & \mathbf{0}_{3\times1}\end{bmatrix}, \tag{76}$$

$$\nabla\mathfrak{L}^2_{\mathbf{g}_{1i}\mathbf{g}_{1j}}\bar{\mathbf{h}}_1 = \frac{\partial\mathfrak{L}^2_{\mathbf{g}_{1i}\mathbf{g}_{1j}}\bar{\mathbf{h}}_1}{\partial\beta} = \mathbf{T}_1\begin{bmatrix}\tilde{\Pi}_{11ij} & \mathbf{0}_{3\times3} & \tilde{\Pi}_{21ij} & \tilde{\Pi}_{31ij} & \tilde{\Pi}_{41ij} & \tilde{\Pi}_{51ij} & \mathbf{0}_{3\times1}\end{bmatrix}, \tag{77}$$

where

$$\tilde{\Pi}_{11ij} = 2\lfloor \mathbf{C}(\beta_4)\mathbf{e}_i \rfloor \lfloor \beta_2 \rfloor \mathbf{C}(\beta_4)\mathbf{e}_j \beta_2^\top + 2\beta_2 (\lfloor \mathbf{C}(\beta_4)\mathbf{e}_i \rfloor \lfloor \beta_2 \rfloor \mathbf{C}(\beta_4)\mathbf{e}_j)^\top - 2\lfloor \beta_2 \rfloor \mathbf{C}(\beta_4)\mathbf{e}_i (\lfloor \beta_2 \rfloor \mathbf{C}(\beta_4)\mathbf{e}_j)^\top - 2\lfloor \beta_2 \rfloor \mathbf{C}(\beta_4)\mathbf{e}_j (\lfloor \beta_2 \rfloor \mathbf{C}(\beta_4)\mathbf{e}_i)^\top, \tag{78}$$

$$\tilde{\Pi}_{31ij} = 2\lfloor \mathbf{C}(\beta_4)\mathbf{e}_i \rfloor \lfloor \beta_2 \rfloor \mathbf{C}(\beta_4)\mathbf{e}_j. \tag{79}$$

APPENDIX B

When the computed gradients of Lie derivatives are stacked together, the observability matrix $\bar{\Xi}$ (a submatrix of Ξ) is constructed as:

$$\bar{\Xi} = \left[\begin{array}{cccccccc}
\mathbf{T}_1(\mathbf{I}_3 - 2\beta_2\beta_2^\top) & \mathbf{0}_{3\times3} & \mathbf{T}_1\Pi_{21} & -2\mathbf{T}_1\beta_2 & -2\mathbf{T}_1\beta_2\beta_2^\top \frac{\partial \mathbf{C}(\beta_4)\beta_5}{\partial \beta_4} & -2\mathbf{T}_1\beta_2\beta_2^\top \mathbf{C}(\beta_4) & \mathbf{0}_{3\times1} \\
\mathbf{0}_{3\times3} & \mathbf{T}_2(\mathbf{I}_3 - 2\beta_2\beta_2^\top) & \mathbf{T}_2\Pi_{22} & -2\mathbf{T}_2\beta_2 & -2\mathbf{T}_2\beta_2\beta_2^\top \frac{\partial \mathbf{C}(\beta_4)\beta_5}{\partial \beta_4} & -2\mathbf{T}_2\beta_2\beta_2^\top \mathbf{C}(\beta_4) & \mathbf{0}_{3\times1} \\
\hline
\mathbf{0}_{3\times3} & \mathbf{0}_{3\times3} & -2\beta_6\mathbf{T}_1 & \mathbf{0}_{3\times3} & \mathbf{0}_{3\times3} & \mathbf{0}_{3\times3} & -2\mathbf{T}_1\beta_2 \\
\hline
-2\mathbf{T}_1(\lfloor\beta_2\rfloor \mathbf{C}(\beta_4)\mathbf{e}_1\beta_2^\top + \beta_2(\lfloor\beta_2\rfloor \mathbf{C}(\beta_4)\mathbf{e}_1)^\top) & \mathbf{0}_{3\times3} & \tilde{\Pi}_{211} & \tilde{\Pi}_{311} & \tilde{\Pi}_{411} & \tilde{\Pi}_{511} & \mathbf{0}_{3\times1} \\
-2\mathbf{T}_1(\lfloor\beta_2\rfloor \mathbf{C}(\beta_4)\mathbf{e}_2\beta_2^\top + \beta_2(\lfloor\beta_2\rfloor \mathbf{C}(\beta_4)\mathbf{e}_2)^\top) & \mathbf{0}_{3\times3} & \tilde{\Pi}_{212} & \tilde{\Pi}_{312} & \tilde{\Pi}_{412} & \tilde{\Pi}_{512} & \mathbf{0}_{3\times1} \\
-2\mathbf{T}_1(\lfloor\beta_2\rfloor \mathbf{C}(\beta_4)\mathbf{e}_3\beta_2^\top + \beta_2(\lfloor\beta_2\rfloor \mathbf{C}(\beta_4)\mathbf{e}_3)^\top) & \mathbf{0}_{3\times3} & \tilde{\Pi}_{213} & \tilde{\Pi}_{313} & \tilde{\Pi}_{413} & \tilde{\Pi}_{513} & \mathbf{0}_{3\times1} \\
\mathbf{0}_{3\times3} & -2\mathbf{T}_2(\lfloor\beta_2\rfloor \mathbf{C}(\beta_4)\mathbf{e}_1\beta_2^\top + \beta_2(\lfloor\beta_2\rfloor \mathbf{C}(\beta_4)\mathbf{e}_1)^\top) & \tilde{\Pi}_{221} & \tilde{\Pi}_{321} & \tilde{\Pi}_{421} & \tilde{\Pi}_{521} & \mathbf{0}_{3\times1} \\
\mathbf{0}_{3\times3} & -2\mathbf{T}_2(\lfloor\beta_2\rfloor \mathbf{C}(\beta_4)\mathbf{e}_2\beta_2^\top + \beta_2(\lfloor\beta_2\rfloor \mathbf{C}(\beta_4)\mathbf{e}_2)^\top) & \tilde{\Pi}_{222} & \tilde{\Pi}_{322} & \tilde{\Pi}_{422} & \tilde{\Pi}_{522} & \mathbf{0}_{3\times1} \\
\mathbf{0}_{3\times3} & -2\mathbf{T}_2(\lfloor\beta_2\rfloor \mathbf{C}(\beta_4)\mathbf{e}_3\beta_2^\top + \beta_2(\lfloor\beta_2\rfloor \mathbf{C}(\beta_4)\mathbf{e}_3)^\top) & \tilde{\Pi}_{223} & \tilde{\Pi}_{323} & \tilde{\Pi}_{423} & \tilde{\Pi}_{523} & \mathbf{0}_{3\times1} \\
\hline
\mathbf{0}_{3\times3} & \mathbf{0}_{3\times3} & 2\beta_6\mathbf{T}_1\lfloor \mathbf{C}(\beta_4)\mathbf{e}_1 \rfloor & \mathbf{0}_{3\times3} & -2\beta_6\mathbf{T}_1\lfloor\beta_2\rfloor \frac{\partial \mathbf{C}(\beta_4)\mathbf{e}_1}{\partial \beta_4} & \mathbf{0}_{3\times3} & -2\mathbf{T}_1\lfloor\beta_2\rfloor \mathbf{C}(\beta_4)\mathbf{e}_1 \\
\mathbf{0}_{3\times3} & \mathbf{0}_{3\times3} & 2\beta_6\mathbf{T}_1\lfloor \mathbf{C}(\beta_4)\mathbf{e}_2 \rfloor & \mathbf{0}_{3\times3} & -2\beta_6\mathbf{T}_1\lfloor\beta_2\rfloor \frac{\partial \mathbf{C}(\beta_4)\mathbf{e}_2}{\partial \beta_4} & \mathbf{0}_{3\times3} & -2\mathbf{T}_1\lfloor\beta_2\rfloor \mathbf{C}(\beta_4)\mathbf{e}_2 \\
\mathbf{0}_{3\times3} & \mathbf{0}_{3\times3} & 2\beta_6\mathbf{T}_1\lfloor \mathbf{C}(\beta_4)\mathbf{e}_3 \rfloor & \mathbf{0}_{3\times3} & -2\beta_6\mathbf{T}_1\lfloor\beta_2\rfloor \frac{\partial \mathbf{C}(\beta_4)\mathbf{e}_3}{\partial \beta_4} & \mathbf{0}_{3\times3} & -2\mathbf{T}_1\lfloor\beta_2\rfloor \mathbf{C}(\beta_4)\mathbf{e}_3 \\
\hline
\mathbf{0}_{3\times3} & \mathbf{0}_{3\times3} & -2\mathbf{T}_1(\beta_2^\top \mathbf{C}(\beta_4)\mathbf{e}_1\mathbf{I}_3 + \beta_2\mathbf{e}_1^\top \mathbf{C}(\beta_4)^\top) & \mathbf{0}_{3\times3} & -2\mathbf{T}_1\beta_2\beta_2^\top \frac{\partial \mathbf{C}(\beta_4)\mathbf{e}_1}{\partial \beta_4} & \mathbf{0}_{3\times3} & \mathbf{0}_{3\times1} \\
\mathbf{0}_{3\times3} & \mathbf{0}_{3\times3} & -2\mathbf{T}_1(\beta_2^\top \mathbf{C}(\beta_4)\mathbf{e}_2\mathbf{I}_3 + \beta_2\mathbf{e}_2^\top \mathbf{C}(\beta_4)^\top) & \mathbf{0}_{3\times3} & -2\mathbf{T}_1\beta_2\beta_2^\top \frac{\partial \mathbf{C}(\beta_4)\mathbf{e}_2}{\partial \beta_4} & \mathbf{0}_{3\times3} & \mathbf{0}_{3\times1} \\
\mathbf{0}_{3\times3} & \mathbf{0}_{3\times3} & -2\mathbf{T}_1(\beta_2^\top \mathbf{C}(\beta_4)\mathbf{e}_3\mathbf{I}_3 + \beta_2\mathbf{e}_3^\top \mathbf{C}(\beta_4)^\top) & \mathbf{0}_{3\times3} & -2\mathbf{T}_1\beta_2\beta_2^\top \frac{\partial \mathbf{C}(\beta_4)\mathbf{e}_3}{\partial \beta_4} & \mathbf{0}_{3\times3} & \mathbf{0}_{3\times1} \\
\mathbf{T}_1\tilde{\Pi}_{1111} & \mathbf{0}_{3\times3} & \mathbf{T}_1\tilde{\Pi}_{2111} & \mathbf{T}_1\tilde{\Pi}_{3111} & \mathbf{T}_1\tilde{\Pi}_{4111} & \tilde{\Pi}_{5111} & \mathbf{0}_{3\times1} \\
\mathbf{T}_1\Pi_{1122} & \mathbf{0}_{3\times3} & \mathbf{T}_1\Pi_{2122} & \mathbf{T}_1\Pi_{3122} & \mathbf{T}_1\Pi_{4122} & \tilde{\Pi}_{5122} & \mathbf{0}_{3\times1} \\
\mathbf{T}_1\tilde{\Pi}_{1133} & \mathbf{0}_{3\times3} & \mathbf{T}_1\tilde{\Pi}_{2133} & \mathbf{T}_1\tilde{\Pi}_{3133} & \mathbf{T}_1\tilde{\Pi}_{4133} & \tilde{\Pi}_{5133} & \mathbf{0}_{3\times1}
\end{array}\right] \tag{80}$$

One way to show that $\bar{\Xi}$ is of full rank is through Gaussian elimination. The Gaussian elimination is performed as follows:

Under the condition that $\beta_6 \neq 0$, we multiply the third block row by $\lfloor \mathbf{C}(\beta_4)\mathbf{e}_i \rfloor$ for $i = \{1,2,3\}$ and when we subtract it from the block rows 10-12, we have

$$\left[\begin{array}{cccccccc}
\mathbf{T}_1(\mathbf{I}_3 - 2\beta_2\beta_2^\top) & \mathbf{0}_{3\times3} & \mathbf{T}_1\Pi_{21} & -2\mathbf{T}_1\beta_2 & -2\mathbf{T}_1\beta_2\beta_2^\top \frac{\partial \mathbf{C}(\beta_4)\beta_5}{\partial \beta_4} & -2\mathbf{T}_1\beta_2\beta_2^\top \mathbf{C}(\beta_4) & \mathbf{0}_{3\times1} \\
\mathbf{0}_{3\times3} & \mathbf{T}_2(\mathbf{I}_3 - 2\beta_2\beta_2^\top) & \mathbf{T}_2\Pi_{22} & -2\mathbf{T}_2\beta_2 & -2\mathbf{T}_2\beta_2\beta_2^\top \frac{\partial \mathbf{C}(\beta_4)\beta_5}{\partial \beta_4} & -2\mathbf{T}_2\beta_2\beta_2^\top \mathbf{C}(\beta_4) & \mathbf{0}_{3\times1} \\
\mathbf{0}_{3\times3} & \mathbf{0}_{3\times3} & -2\beta_6\mathbf{T}_1 & \mathbf{0}_{3\times3} & \mathbf{0}_{3\times3} & \mathbf{0}_{3\times3} & -2\mathbf{T}_1\beta_2 \\
-2\mathbf{T}_1(\lfloor\beta_2\rfloor \mathbf{C}(\beta_4)\mathbf{e}_1\beta_2^\top + \beta_2(\lfloor\beta_2\rfloor \mathbf{C}(\beta_4)\mathbf{e}_1)^\top) & \mathbf{0}_{3\times3} & \tilde{\Pi}_{211} & \tilde{\Pi}_{311} & \tilde{\Pi}_{411} & \tilde{\Pi}_{511} & \mathbf{0}_{3\times1} \\
-2\mathbf{T}_1(\lfloor\beta_2\rfloor \mathbf{C}(\beta_4)\mathbf{e}_2\beta_2^\top + \beta_2(\lfloor\beta_2\rfloor \mathbf{C}(\beta_4)\mathbf{e}_2)^\top) & \mathbf{0}_{3\times3} & \tilde{\Pi}_{212} & \tilde{\Pi}_{312} & \tilde{\Pi}_{412} & \tilde{\Pi}_{512} & \mathbf{0}_{3\times1} \\
-2\mathbf{T}_1(\lfloor\beta_2\rfloor \mathbf{C}(\beta_4)\mathbf{e}_3\beta_2^\top + \beta_2(\lfloor\beta_2\rfloor \mathbf{C}(\beta_4)\mathbf{e}_3)^\top) & \mathbf{0}_{3\times3} & \tilde{\Pi}_{213} & \tilde{\Pi}_{313} & \tilde{\Pi}_{413} & \tilde{\Pi}_{513} & \mathbf{0}_{3\times1} \\
\mathbf{0}_{3\times3} & -2\mathbf{T}_2(\lfloor\beta_2\rfloor \mathbf{C}(\beta_4)\mathbf{e}_1\beta_2^\top + \beta_2(\lfloor\beta_2\rfloor \mathbf{C}(\beta_4)\mathbf{e}_1)^\top) & \tilde{\Pi}_{221} & \tilde{\Pi}_{321} & \tilde{\Pi}_{421} & \tilde{\Pi}_{521} & \mathbf{0}_{3\times1} \\
\mathbf{0}_{3\times3} & -2\mathbf{T}_2(\lfloor\beta_2\rfloor \mathbf{C}(\beta_4)\mathbf{e}_2\beta_2^\top + \beta_2(\lfloor\beta_2\rfloor \mathbf{C}(\beta_4)\mathbf{e}_2)^\top) & \tilde{\Pi}_{222} & \tilde{\Pi}_{322} & \tilde{\Pi}_{422} & \tilde{\Pi}_{522} & \mathbf{0}_{3\times1} \\
\mathbf{0}_{3\times3} & -2\mathbf{T}_2(\lfloor\beta_2\rfloor \mathbf{C}(\beta_4)\mathbf{e}_3\beta_2^\top + \beta_2(\lfloor\beta_2\rfloor \mathbf{C}(\beta_4)\mathbf{e}_3)^\top) & \tilde{\Pi}_{223} & \tilde{\Pi}_{323} & \tilde{\Pi}_{423} & \tilde{\Pi}_{523} & \mathbf{0}_{3\times1} \\
\hline
\mathbf{0}_{3\times3} & \mathbf{0}_{3\times3} & \mathbf{0}_{3\times3} & \mathbf{0}_{3\times3} & -2\beta_6\mathbf{T}_1\lfloor\beta_2\rfloor \frac{\partial \mathbf{C}(\beta_4)\mathbf{e}_1}{\partial \beta_4} & \mathbf{0}_{3\times3} & \mathbf{0}_{3\times1} \\
\mathbf{0}_{3\times3} & \mathbf{0}_{3\times3} & \mathbf{0}_{3\times3} & \mathbf{0}_{3\times3} & -2\beta_6\mathbf{T}_1\lfloor\beta_2\rfloor \frac{\partial \mathbf{C}(\beta_4)\mathbf{e}_2}{\partial \beta_4} & \mathbf{0}_{3\times3} & \mathbf{0}_{3\times1} \\
\mathbf{0}_{3\times3} & \mathbf{0}_{3\times3} & \mathbf{0}_{3\times3} & \mathbf{0}_{3\times3} & -2\beta_6\mathbf{T}_1\lfloor\beta_2\rfloor \frac{\partial \mathbf{C}(\beta_4)\mathbf{e}_3}{\partial \beta_4} & \mathbf{0}_{3\times3} & \mathbf{0}_{3\times1} \\
\hline
\mathbf{0}_{3\times3} & \mathbf{0}_{3\times3} & -2\mathbf{T}_1(\beta_2^\top \mathbf{C}(\beta_4)\mathbf{e}_1\mathbf{I}_3 + \beta_2\mathbf{e}_1^\top \mathbf{C}(\beta_4)^\top) & \mathbf{0}_{3\times3} & -2\mathbf{T}_1\beta_2\beta_2^\top \frac{\partial \mathbf{C}(\beta_4)\mathbf{e}_1}{\partial \beta_4} & \mathbf{0}_{3\times3} & \mathbf{0}_{3\times1} \\
\mathbf{0}_{3\times3} & \mathbf{0}_{3\times3} & -2\mathbf{T}_1(\beta_2^\top \mathbf{C}(\beta_4)\mathbf{e}_2\mathbf{I}_3 + \beta_2\mathbf{e}_2^\top \mathbf{C}(\beta_4)^\top) & \mathbf{0}_{3\times3} & -2\mathbf{T}_1\beta_2\beta_2^\top \frac{\partial \mathbf{C}(\beta_4)\mathbf{e}_2}{\partial \beta_4} & \mathbf{0}_{3\times3} & \mathbf{0}_{3\times1} \\
\mathbf{0}_{3\times3} & \mathbf{0}_{3\times3} & -2\mathbf{T}_1(\beta_2^\top \mathbf{C}(\beta_4)\mathbf{e}_3\mathbf{I}_3 + \beta_2\mathbf{e}_3^\top \mathbf{C}(\beta_4)^\top) & \mathbf{0}_{3\times3} & -2\mathbf{T}_1\beta_2\beta_2^\top \frac{\partial \mathbf{C}(\beta_4)\mathbf{e}_3}{\partial \beta_4} & \mathbf{0}_{3\times3} & \mathbf{0}_{3\times1} \\
\mathbf{T}_1\tilde{\Pi}_{1111} & \mathbf{0}_{3\times3} & \mathbf{T}_1\tilde{\Pi}_{2111} & \mathbf{T}_1\tilde{\Pi}_{3111} & \mathbf{T}_1\tilde{\Pi}_{4111} & \tilde{\Pi}_{5111} & \mathbf{0}_{3\times1} \\
\mathbf{T}_1\Pi_{1122} & \mathbf{0}_{3\times3} & \mathbf{T}_1\Pi_{2122} & \mathbf{T}_1\Pi_{3122} & \mathbf{T}_1\Pi_{4122} & \tilde{\Pi}_{5122} & \mathbf{0}_{3\times1} \\
\mathbf{T}_1\tilde{\Pi}_{1133} & \mathbf{0}_{3\times3} & \mathbf{T}_1\tilde{\Pi}_{2133} & \mathbf{T}_1\tilde{\Pi}_{3133} & \mathbf{T}_1\tilde{\Pi}_{4133} & \tilde{\Pi}_{5133} & \mathbf{0}_{3\times1}
\end{array}\right]. \tag{81}$$

The non-zero terms that remain between block rows 10-12 can be represented in matrix form as:

$$\left[\begin{array}{c}
-2\beta_6\mathbf{T}_1\lfloor\beta_2\rfloor \frac{\partial \mathbf{C}(\beta_4)\mathbf{e}_1}{\partial \beta_4} \\
-2\beta_6\mathbf{T}_1\lfloor\beta_2\rfloor \frac{\partial \mathbf{C}(\beta_4)\mathbf{e}_2}{\partial \beta_4} \\
-2\beta_6\mathbf{T}_1\lfloor\beta_2\rfloor \frac{\partial \mathbf{C}(\beta_4)\mathbf{e}_3}{\partial \beta_4}
\end{array}\right], \tag{82}$$

which is of full column rank. Hence, it can be used to eliminate all the other terms in the fifth block column:

$$\left[\begin{array}{ccccccc}
\mathbf{T}_1(\mathbf{I}_3-2\beta_2\beta_2^\top) & \mathbf{0}_{3\times3} & \mathbf{T}_1\Pi_{21} & -2\mathbf{T}_1\beta_2 & \mathbf{0}_{3\times3} & -2\mathbf{T}_1\beta_2\beta_2^\top\mathbf{C}(\beta_4) & \mathbf{0}_{3\times1}\\
\mathbf{0}_{3\times3} & \mathbf{T}_2(\mathbf{I}_3-2\beta_2\beta_2^\top) & \mathbf{T}_2\Pi_{22} & -2\mathbf{T}_2\beta_2 & \mathbf{0}_{3\times3} & -2\mathbf{T}_2\beta_2\beta_2^\top\mathbf{C}(\beta_4) & \mathbf{0}_{3\times1}\\
\mathbf{0}_{3\times3} & \mathbf{0}_{3\times3} & -2\beta_6\mathbf{T}_1 & \mathbf{0}_{3\times3} & \mathbf{0}_{3\times3} & \mathbf{0}_{3\times3} & -2\mathbf{T}_1\beta_2\\
-2\mathbf{T}_1(\lfloor\beta_2\rfloor\mathbf{C}(\beta_4)\mathbf{e}_1\beta_2^\top+\beta_2(\lfloor\beta_2\rfloor\mathbf{C}(\beta_4)\mathbf{e}_1)^\top) & \mathbf{0}_{3\times3} & \tilde{\Pi}_{211} & \tilde{\Pi}_{311} & \mathbf{0}_{3\times3} & \tilde{\Pi}_{511} & \mathbf{0}_{3\times1}\\
-2\mathbf{T}_1(\lfloor\beta_2\rfloor\mathbf{C}(\beta_4)\mathbf{e}_2\beta_2^\top+\beta_2(\lfloor\beta_2\rfloor\mathbf{C}(\beta_4)\mathbf{e}_2)^\top) & \mathbf{0}_{3\times3} & \tilde{\Pi}_{212} & \tilde{\Pi}_{312} & \mathbf{0}_{3\times3} & \tilde{\Pi}_{512} & \mathbf{0}_{3\times1}\\
-2\mathbf{T}_1(\lfloor\beta_2\rfloor\mathbf{C}(\beta_4)\mathbf{e}_3\beta_2^\top+\beta_2(\lfloor\beta_2\rfloor\mathbf{C}(\beta_4)\mathbf{e}_3)^\top) & \mathbf{0}_{3\times3} & \tilde{\Pi}_{213} & \tilde{\Pi}_{313} & \mathbf{0}_{3\times3} & \tilde{\Pi}_{513} & \mathbf{0}_{3\times1}\\
\mathbf{0}_{3\times3} & -2\mathbf{T}_2(\lfloor\beta_2\rfloor\mathbf{C}(\beta_4)\mathbf{e}_1\beta_2^\top+\beta_2(\lfloor\beta_2\rfloor\mathbf{C}(\beta_4)\mathbf{e}_1)^\top) & \tilde{\Pi}_{221} & \tilde{\Pi}_{321} & \mathbf{0}_{3\times3} & \tilde{\Pi}_{521} & \mathbf{0}_{3\times1}\\
\mathbf{0}_{3\times3} & -2\mathbf{T}_2(\lfloor\beta_2\rfloor\mathbf{C}(\beta_4)\mathbf{e}_2\beta_2^\top+\beta_2(\lfloor\beta_2\rfloor\mathbf{C}(\beta_4)\mathbf{e}_2)^\top) & \tilde{\Pi}_{222} & \tilde{\Pi}_{322} & \mathbf{0}_{3\times3} & \tilde{\Pi}_{522} & \mathbf{0}_{3\times1}\\
\mathbf{0}_{3\times3} & -2\mathbf{T}_2(\lfloor\beta_2\rfloor\mathbf{C}(\beta_4)\mathbf{e}_3\beta_2^\top+\beta_2(\lfloor\beta_2\rfloor\mathbf{C}(\beta_4)\mathbf{e}_3)^\top) & \tilde{\Pi}_{223} & \tilde{\Pi}_{323} & \mathbf{0}_{3\times3} & \tilde{\Pi}_{523} & \mathbf{0}_{3\times1}\\
\mathbf{0}_{3\times3} & \mathbf{0}_{3\times3} & \mathbf{0}_{3\times1} & \mathbf{0}_{3\times3} & \mathbf{I}_3 & \mathbf{0}_{3\times3} & \mathbf{0}_{3\times1}\\
\hline
\mathbf{0}_{3\times3} & \mathbf{0}_{3\times3} & -2\mathbf{T}_1(\beta_2^\top\mathbf{C}(\beta_4)\mathbf{e}_1\mathbf{I}_3+\beta_2\mathbf{e}_1^\top\mathbf{C}(\beta_4)^\top) & \mathbf{0}_{3\times3} & \mathbf{0}_{3\times3} & \mathbf{0}_{3\times3} & \mathbf{0}_{3\times1}\\
\mathbf{0}_{3\times3} & \mathbf{0}_{3\times3} & -2\mathbf{T}_1(\beta_2^\top\mathbf{C}(\beta_4)\mathbf{e}_2\mathbf{I}_3+\beta_2\mathbf{e}_2^\top\mathbf{C}(\beta_4)^\top) & \mathbf{0}_{3\times3} & \mathbf{0}_{3\times3} & \mathbf{0}_{3\times3} & \mathbf{0}_{3\times1}\\
\mathbf{0}_{3\times3} & \mathbf{0}_{3\times3} & -2\mathbf{T}_1(\beta_2^\top\mathbf{C}(\beta_4)\mathbf{e}_3\mathbf{I}_3+\beta_2\mathbf{e}_3^\top\mathbf{C}(\beta_4)^\top) & \mathbf{0}_{3\times3} & \mathbf{0}_{3\times3} & \mathbf{0}_{3\times3} & \mathbf{0}_{3\times1}\\
\hline
\mathbf{T}_1\tilde{\Pi}_{1111} & \mathbf{0}_{3\times3} & \mathbf{T}_1\tilde{\Pi}_{2111} & \mathbf{T}_1\tilde{\Pi}_{3111} & \mathbf{0}_{3\times3} & \tilde{\Pi}_{5111} & \mathbf{0}_{3\times1}\\
\mathbf{T}_1\Pi_{1122} & \mathbf{0}_{3\times3} & \mathbf{T}_1\Pi_{2122} & \mathbf{T}_1\Pi_{3122} & \mathbf{0}_{3\times3} & \Pi_{5122} & \mathbf{0}_{3\times1}\\
\mathbf{T}_1\tilde{\Pi}_{1133} & \mathbf{0}_{3\times3} & \mathbf{T}_1\tilde{\Pi}_{2133} & \mathbf{T}_1\tilde{\Pi}_{3133} & \mathbf{0}_{3\times3} & \tilde{\Pi}_{5133} & \mathbf{0}_{3\times1}
\end{array}\right]. \quad (83)$$

The non-zero terms in the specified block row in the third column in the matrix form are

$$\left[\begin{array}{c}
-2\mathbf{T}_1(\beta_2^\top\mathbf{C}(\beta_4)\mathbf{e}_1\mathbf{I}_3+\beta_2\mathbf{e}_1^\top\mathbf{C}(\beta_4)^\top)\\
-2\mathbf{T}_1(\beta_2^\top\mathbf{C}(\beta_4)\mathbf{e}_2\mathbf{I}_3+\beta_2\mathbf{e}_2^\top\mathbf{C}(\beta_4)^\top)\\
-2\mathbf{T}_1(\beta_2^\top\mathbf{C}(\beta_4)\mathbf{e}_3\mathbf{I}_3+\beta_2\mathbf{e}_3^\top\mathbf{C}(\beta_4)^\top)
\end{array}\right], \quad (84)$$

which is of full rank, so it can be used to eliminate all the other terms in the third block column. Then we have

$$\left[\begin{array}{ccccccc}
\mathbf{T}_1(\mathbf{I}_3-2\beta_2\beta_2^\top) & \mathbf{0}_{3\times3} & \mathbf{0}_{3\times3} & -2\mathbf{T}_1\beta_2 & \mathbf{0}_{3\times3} & -2\mathbf{T}_1\beta_2\beta_2^\top\mathbf{C}(\beta_4) & \mathbf{0}_{3\times1}\\
\mathbf{0}_{3\times3} & \mathbf{T}_2(\mathbf{I}_3-2\beta_2\beta_2^\top) & \mathbf{0}_{3\times3} & -2\mathbf{T}_2\beta_2 & \mathbf{0}_{3\times3} & -2\mathbf{T}_2\beta_2\beta_2^\top\mathbf{C}(\beta_4) & \mathbf{0}_{3\times1}\\
\mathbf{0}_{3\times3} & \mathbf{0}_{3\times3} & \mathbf{0}_{3\times3} & \mathbf{0}_{3\times1} & \mathbf{0}_{3\times3} & \mathbf{0}_{3\times3} & -2\mathbf{T}_1\beta_2\\
-2\mathbf{T}_1(\lfloor\beta_2\rfloor\mathbf{C}(\beta_4)\mathbf{e}_1\beta_2^\top+\beta_2(\lfloor\beta_2\rfloor\mathbf{C}(\beta_4)\mathbf{e}_1)^\top) & \mathbf{0}_{3\times3} & \mathbf{0}_{3\times3} & \tilde{\Pi}_{311} & \mathbf{0}_{3\times3} & \tilde{\Pi}_{511} & \mathbf{0}_{3\times1}\\
-2\mathbf{T}_1(\lfloor\beta_2\rfloor\mathbf{C}(\beta_4)\mathbf{e}_2\beta_2^\top+\beta_2(\lfloor\beta_2\rfloor\mathbf{C}(\beta_4)\mathbf{e}_2)^\top) & \mathbf{0}_{3\times3} & \mathbf{0}_{3\times3} & \tilde{\Pi}_{312} & \mathbf{0}_{3\times3} & \tilde{\Pi}_{512} & \mathbf{0}_{3\times1}\\
-2\mathbf{T}_1(\lfloor\beta_2\rfloor\mathbf{C}(\beta_4)\mathbf{e}_3\beta_2^\top+\beta_2(\lfloor\beta_2\rfloor\mathbf{C}(\beta_4)\mathbf{e}_3)^\top) & \mathbf{0}_{3\times3} & \mathbf{0}_{3\times3} & \tilde{\Pi}_{313} & \mathbf{0}_{3\times3} & \tilde{\Pi}_{513} & \mathbf{0}_{3\times1}\\
\mathbf{0}_{3\times3} & -2\mathbf{T}_2(\lfloor\beta_2\rfloor\mathbf{C}(\beta_4)\mathbf{e}_1\beta_2^\top+\beta_2(\lfloor\beta_2\rfloor\mathbf{C}(\beta_4)\mathbf{e}_1)^\top) & \mathbf{0}_{3\times3} & \tilde{\Pi}_{321} & \mathbf{0}_{3\times3} & \tilde{\Pi}_{521} & \mathbf{0}_{3\times1}\\
\mathbf{0}_{3\times3} & -2\mathbf{T}_2(\lfloor\beta_2\rfloor\mathbf{C}(\beta_4)\mathbf{e}_2\beta_2^\top+\beta_2(\lfloor\beta_2\rfloor\mathbf{C}(\beta_4)\mathbf{e}_2)^\top) & \mathbf{0}_{3\times3} & \tilde{\Pi}_{322} & \mathbf{0}_{3\times3} & \tilde{\Pi}_{522} & \mathbf{0}_{3\times1}\\
\mathbf{0}_{3\times3} & -2\mathbf{T}_2(\lfloor\beta_2\rfloor\mathbf{C}(\beta_4)\mathbf{e}_3\beta_2^\top+\beta_2(\lfloor\beta_2\rfloor\mathbf{C}(\beta_4)\mathbf{e}_3)^\top) & \mathbf{0}_{3\times3} & \tilde{\Pi}_{323} & \mathbf{0}_{3\times3} & \tilde{\Pi}_{523} & \mathbf{0}_{3\times1}\\
\mathbf{0}_{3\times3} & \mathbf{0}_{3\times3} & \mathbf{0}_{3\times3} & \mathbf{0}_{3\times3} & \mathbf{I}_3 & \mathbf{0}_{3\times3} & \mathbf{0}_{3\times1}\\
\mathbf{0}_{3\times3} & \mathbf{0}_{3\times3} & \mathbf{I}_3 & \mathbf{0}_{3\times3} & \mathbf{0}_{3\times3} & \mathbf{0}_{3\times3} & \mathbf{0}_{3\times1}\\
\mathbf{T}_1\tilde{\Pi}_{1111} & \mathbf{0}_{3\times3} & \mathbf{0}_{3\times3} & \mathbf{T}_1\tilde{\Pi}_{3111} & \mathbf{0}_{3\times3} & \tilde{\Pi}_{5111} & \mathbf{0}_{3\times1}\\
\mathbf{T}_1\Pi_{1122} & \mathbf{0}_{3\times3} & \mathbf{0}_{3\times3} & \mathbf{T}_1\Pi_{3122} & \mathbf{0}_{3\times3} & \Pi_{5122} & \mathbf{0}_{3\times1}\\
\mathbf{T}_1\tilde{\Pi}_{1133} & \mathbf{0}_{3\times3} & \mathbf{0}_{3\times3} & \mathbf{T}_1\tilde{\Pi}_{3133} & \mathbf{0}_{3\times3} & \tilde{\Pi}_{5133} & \mathbf{0}_{3\times1}
\end{array}\right]. \quad (85)$$

When the sixth block column is multiplied with $\mathbf{C}(\beta_4)^\top$ (a full rank matrix) and then the first and second block columns are subtracted from it, we have

$$\left[\begin{array}{ccccccc}
\mathbf{T}_1(\mathbf{I}_3-2\beta_2\beta_2^\top) & \mathbf{0}_{3\times3} & \mathbf{0}_{3\times3} & -2\mathbf{T}_1\beta_2 & \mathbf{0}_{3\times3} & \mathbf{T}_1 & \mathbf{0}_{3\times1}\\
\mathbf{0}_{3\times3} & \mathbf{T}_2(\mathbf{I}_3-2\beta_2\beta_2^\top) & \mathbf{0}_{3\times3} & -2\mathbf{T}_2\beta_2 & \mathbf{0}_{3\times3} & \mathbf{T}_2 & \mathbf{0}_{3\times1}\\
\mathbf{0}_{3\times3} & \mathbf{0}_{3\times3} & \mathbf{0}_{3\times3} & \mathbf{0}_{3\times1} & \mathbf{0}_{3\times3} & \mathbf{0}_{3\times3} & -2\mathbf{T}_1\beta_2\\
-2\mathbf{T}_1(\lfloor\beta_2\rfloor\mathbf{C}(\beta_4)\mathbf{e}_1\beta_2^\top+\beta_2(\lfloor\beta_2\rfloor\mathbf{C}(\beta_4)\mathbf{e}_1)^\top) & \mathbf{0}_{3\times3} & \mathbf{0}_{3\times3} & \tilde{\Pi}_{311} & \mathbf{0}_{3\times3} & \mathbf{0}_{3\times3} & \mathbf{0}_{3\times1}\\
-2\mathbf{T}_1(\lfloor\beta_2\rfloor\mathbf{C}(\beta_4)\mathbf{e}_2\beta_2^\top+\beta_2(\lfloor\beta_2\rfloor\mathbf{C}(\beta_4)\mathbf{e}_2)^\top) & \mathbf{0}_{3\times3} & \mathbf{0}_{3\times3} & \tilde{\Pi}_{312} & \mathbf{0}_{3\times3} & \mathbf{0}_{3\times3} & \mathbf{0}_{3\times1}\\
-2\mathbf{T}_1(\lfloor\beta_2\rfloor\mathbf{C}(\beta_4)\mathbf{e}_3\beta_2^\top+\beta_2(\lfloor\beta_2\rfloor\mathbf{C}(\beta_4)\mathbf{e}_3)^\top) & \mathbf{0}_{3\times3} & \mathbf{0}_{3\times3} & \tilde{\Pi}_{313} & \mathbf{0}_{3\times3} & \mathbf{0}_{3\times3} & \mathbf{0}_{3\times1}\\
\mathbf{0}_{3\times3} & -2\mathbf{T}_2(\lfloor\beta_2\rfloor\mathbf{C}(\beta_4)\mathbf{e}_1\beta_2^\top+\beta_2(\lfloor\beta_2\rfloor\mathbf{C}(\beta_4)\mathbf{e}_1)^\top) & \mathbf{0}_{3\times3} & \tilde{\Pi}_{321} & \mathbf{0}_{3\times3} & \mathbf{0}_{3\times3} & \mathbf{0}_{3\times1}\\
\mathbf{0}_{3\times3} & -2\mathbf{T}_2(\lfloor\beta_2\rfloor\mathbf{C}(\beta_4)\mathbf{e}_2\beta_2^\top+\beta_2(\lfloor\beta_2\rfloor\mathbf{C}(\beta_4)\mathbf{e}_2)^\top) & \mathbf{0}_{3\times3} & \tilde{\Pi}_{322} & \mathbf{0}_{3\times3} & \mathbf{0}_{3\times3} & \mathbf{0}_{3\times1}\\
\mathbf{0}_{3\times3} & -2\mathbf{T}_2(\lfloor\beta_2\rfloor\mathbf{C}(\beta_4)\mathbf{e}_3\beta_2^\top+\beta_2(\lfloor\beta_2\rfloor\mathbf{C}(\beta_4)\mathbf{e}_3)^\top) & \mathbf{0}_{3\times3} & \tilde{\Pi}_{323} & \mathbf{0}_{3\times3} & \mathbf{0}_{3\times3} & \mathbf{0}_{3\times1}\\
\mathbf{0}_{3\times3} & \mathbf{0}_{3\times3} & \mathbf{0}_{3\times3} & \mathbf{0}_{3\times3} & \mathbf{I}_3 & \mathbf{0}_{3\times3} & \mathbf{0}_{3\times1}\\
\mathbf{0}_{3\times3} & \mathbf{0}_{3\times3} & \mathbf{I}_3 & \mathbf{0}_{3\times3} & \mathbf{0}_{3\times3} & \mathbf{0}_{3\times3} & \mathbf{0}_{3\times1}\\
\mathbf{T}_1\tilde{\Pi}_{1111} & \mathbf{0}_{3\times3} & \mathbf{0}_{3\times3} & \mathbf{T}_1\tilde{\Pi}_{3111} & \mathbf{0}_{3\times3} & \mathbf{0}_{3\times3} & \mathbf{0}_{3\times1}\\
\mathbf{T}_1\Pi_{1122} & \mathbf{0}_{3\times3} & \mathbf{0}_{3\times3} & \mathbf{T}_1\Pi_{3122} & \mathbf{0}_{3\times3} & \mathbf{0}_{3\times3} & \mathbf{0}_{3\times1}\\
\mathbf{T}_1\tilde{\Pi}_{1133} & \mathbf{0}_{3\times3} & \mathbf{0}_{3\times3} & \mathbf{T}_1\tilde{\Pi}_{3133} & \mathbf{0}_{3\times3} & \mathbf{0}_{3\times3} & \mathbf{0}_{3\times1}
\end{array}\right]. \quad (86)$$

When the first and second block columns are multiplied with β_2 and then subtracted from the fourth block column, we get

$$\left[\begin{array}{ccccccc}
\mathbf{T}_1(\mathbf{I}_3-2\beta_2\beta_2^\top) & \mathbf{0}_{3\times3} & \mathbf{0}_{3\times3} & -2\mathbf{T}_1\beta_2 & \mathbf{0}_{3\times3} & \mathbf{T}_1 & \mathbf{0}_{3\times1}\\
\mathbf{0}_{3\times3} & \mathbf{T}_2(\mathbf{I}_3-2\beta_2\beta_2^\top) & \mathbf{0}_{3\times3} & -2\mathbf{T}_2\beta_2 & \mathbf{0}_{3\times3} & \mathbf{T}_2 & \mathbf{0}_{3\times1}\\
\mathbf{0}_{3\times3} & \mathbf{0}_{3\times3} & \mathbf{0}_{3\times3} & \mathbf{0}_{3\times1} & \mathbf{0}_{3\times3} & \mathbf{0}_{3\times3} & -2\mathbf{T}_1\beta_2\\
-2\mathbf{T}_1(\lfloor\beta_2\rfloor\mathbf{C}(\beta_4)\mathbf{e}_1\beta_2^\top+\beta_2(\lfloor\beta_2\rfloor\mathbf{C}(\beta_4)\mathbf{e}_1)^\top) & \mathbf{0}_{3\times3} & \mathbf{0}_{3\times3} & \mathbf{0}_{3\times1} & \mathbf{0}_{3\times3} & \mathbf{0}_{3\times3} & \mathbf{0}_{3\times1}\\
-2\mathbf{T}_1(\lfloor\beta_2\rfloor\mathbf{C}(\beta_4)\mathbf{e}_2\beta_2^\top+\beta_2(\lfloor\beta_2\rfloor\mathbf{C}(\beta_4)\mathbf{e}_2)^\top) & \mathbf{0}_{3\times3} & \mathbf{0}_{3\times3} & \mathbf{0}_{3\times1} & \mathbf{0}_{3\times3} & \mathbf{0}_{3\times3} & \mathbf{0}_{3\times1}\\
-2\mathbf{T}_1(\lfloor\beta_2\rfloor\mathbf{C}(\beta_4)\mathbf{e}_3\beta_2^\top+\beta_2(\lfloor\beta_2\rfloor\mathbf{C}(\beta_4)\mathbf{e}_3)^\top) & \mathbf{0}_{3\times3} & \mathbf{0}_{3\times3} & \mathbf{0}_{3\times1} & \mathbf{0}_{3\times3} & \mathbf{0}_{3\times3} & \mathbf{0}_{3\times1}\\
\mathbf{0}_{3\times3} & -2\mathbf{T}_2(\lfloor\beta_2\rfloor\mathbf{C}(\beta_4)\mathbf{e}_1\beta_2^\top+\beta_2(\lfloor\beta_2\rfloor\mathbf{C}(\beta_4)\mathbf{e}_1)^\top) & \mathbf{0}_{3\times3} & \mathbf{0}_{3\times1} & \mathbf{0}_{3\times3} & \mathbf{0}_{3\times3} & \mathbf{0}_{3\times1}\\
\mathbf{0}_{3\times3} & -2\mathbf{T}_2(\lfloor\beta_2\rfloor\mathbf{C}(\beta_4)\mathbf{e}_2\beta_2^\top+\beta_2(\lfloor\beta_2\rfloor\mathbf{C}(\beta_4)\mathbf{e}_2)^\top) & \mathbf{0}_{3\times3} & \mathbf{0}_{3\times1} & \mathbf{0}_{3\times3} & \mathbf{0}_{3\times3} & \mathbf{0}_{3\times1}\\
\mathbf{0}_{3\times3} & -2\mathbf{T}_2(\lfloor\beta_2\rfloor\mathbf{C}(\beta_4)\mathbf{e}_3\beta_2^\top+\beta_2(\lfloor\beta_2\rfloor\mathbf{C}(\beta_4)\mathbf{e}_3)^\top) & \mathbf{0}_{3\times3} & \mathbf{0}_{3\times1} & \mathbf{0}_{3\times3} & \mathbf{0}_{3\times3} & \mathbf{0}_{3\times1}\\
\mathbf{0}_{3\times3} & \mathbf{0}_{3\times3} & \mathbf{0}_{3\times3} & \mathbf{0}_{3\times1} & \mathbf{I}_3 & \mathbf{0}_{3\times3} & \mathbf{0}_{3\times1}\\
\mathbf{0}_{3\times3} & \mathbf{0}_{3\times3} & \mathbf{I}_3 & \mathbf{0}_{3\times1} & \mathbf{0}_{3\times3} & \mathbf{0}_{3\times3} & \mathbf{0}_{3\times1}\\
\mathbf{T}_1\tilde{\Pi}_{1111} & \mathbf{0}_{3\times3} & \mathbf{0}_{3\times3} & 2\mathbf{T}_1\beta_2(\lfloor\mathbf{C}(\beta_4)\mathbf{e}_1\rfloor\lfloor\beta_2\rfloor\mathbf{C}(\beta_4)\mathbf{e}_1)^\top\beta_2 & \mathbf{0}_{3\times3} & \mathbf{0}_{3\times3} & \mathbf{0}_{3\times1}\\
\mathbf{T}_1\Pi_{1122} & \mathbf{0}_{3\times3} & \mathbf{0}_{3\times3} & 2\mathbf{T}_1\beta_2(\lfloor\mathbf{C}(\beta_4)\mathbf{e}_2\rfloor\lfloor\beta_2\rfloor\mathbf{C}(\beta_4)\mathbf{e}_2)^\top\beta_2 & \mathbf{0}_{3\times3} & \mathbf{0}_{3\times3} & \mathbf{0}_{3\times1}\\
\mathbf{T}_1\tilde{\Pi}_{1133} & \mathbf{0}_{3\times3} & \mathbf{0}_{3\times3} & 2\mathbf{T}_1\beta_2(\lfloor\mathbf{C}(\beta_4)\mathbf{e}_3\rfloor\lfloor\beta_2\rfloor\mathbf{C}(\beta_4)\mathbf{e}_3)^\top\beta_2 & \mathbf{0}_{3\times3} & \mathbf{0}_{3\times3} & \mathbf{0}_{3\times1}
\end{array}\right]. \quad (87)$$

The non-zero block matrices in the first and second block columns are of full column rank, and can be used to eliminate the non-zero terms in their corresponding block columns as

$$\begin{bmatrix} \mathbf{0}_{3\times3} & \mathbf{0}_{3\times3} & \mathbf{0}_{3\times3} & -2\mathbf{T}_1\beta_2 & \mathbf{0}_{3\times3} & \mathbf{T}_1 & \mathbf{0}_{3\times1} \\ \mathbf{0}_{3\times3} & \mathbf{0}_{3\times3} & \mathbf{0}_{3\times3} & -2\mathbf{T}_2\beta_2 & \mathbf{0}_{3\times3} & \mathbf{T}_2 & \mathbf{0}_{3\times1} \\ \mathbf{0}_{3\times3} & \mathbf{0}_{3\times3} & \mathbf{0}_{3\times3} & \mathbf{0}_{3\times1} & \mathbf{0}_{3\times3} & \mathbf{0}_{3\times3} & -2\mathbf{T}_1\beta_2 \\ \mathbf{I}_3 & \mathbf{0}_{3\times3} & \mathbf{0}_{3\times3} & \mathbf{0}_{3\times1} & \mathbf{0}_{3\times3} & \mathbf{0}_{3\times3} & \mathbf{0}_{3\times1} \\ \mathbf{0}_{3\times3} & \mathbf{I}_3 & \mathbf{0}_{3\times3} & \mathbf{0}_{3\times1} & \mathbf{0}_{3\times3} & \mathbf{0}_{3\times3} & \mathbf{0}_{3\times1} \\ \mathbf{0}_{3\times3} & \mathbf{0}_{3\times3} & \mathbf{0}_{3\times3} & \mathbf{0}_{3\times1} & \mathbf{I}_3 & \mathbf{0}_{3\times3} & \mathbf{0}_{3\times1} \\ \mathbf{0}_{3\times3} & \mathbf{0}_{3\times3} & \mathbf{I}_3 & \mathbf{0}_{3\times1} & \mathbf{0}_{3\times3} & \mathbf{0}_{3\times3} & \mathbf{0}_{3\times1} \\ \mathbf{0}_{3\times3} & \mathbf{0}_{3\times3} & \mathbf{0}_{3\times3} & 2\mathbf{T}_1\beta_2\left(\lfloor\mathbf{C}(\beta_4)\mathbf{e}_1\rfloor\lfloor\beta_2\rfloor\mathbf{C}(\beta_4)\mathbf{e}_1\right)^\top\beta_2 & \mathbf{0}_{3\times3} & \mathbf{0}_{3\times3} & \mathbf{0}_{3\times1} \\ \mathbf{0}_{3\times3} & \mathbf{0}_{3\times3} & \mathbf{0}_{3\times3} & 2\mathbf{T}_1\beta_2\left(\lfloor\mathbf{C}(\beta_4)\mathbf{e}_2\rfloor\lfloor\beta_2\rfloor\mathbf{C}(\beta_4)\mathbf{e}_2\right)^\top\beta_2 & \mathbf{0}_{3\times3} & \mathbf{0}_{3\times3} & \mathbf{0}_{3\times1} \\ \mathbf{0}_{3\times3} & \mathbf{0}_{3\times3} & \mathbf{0}_{3\times3} & 2\mathbf{T}_1\beta_2\left(\lfloor\mathbf{C}(\beta_4)\mathbf{e}_3\rfloor\lfloor\beta_2\rfloor\mathbf{C}(\beta_4)\mathbf{e}_3\right)^\top\beta_2 & \mathbf{0}_{3\times3} & \mathbf{0}_{3\times3} & \mathbf{0}_{3\times1} \end{bmatrix}. \tag{88}$$

The non-zero terms in the last three block rows form a matrix that is of full column rank, and can be used to eliminate the other terms in the fourth block column:

$$\begin{bmatrix} \mathbf{0}_{3\times3} & \mathbf{0}_{3\times3} & \mathbf{0}_{3\times3} & \mathbf{0}_{3\times1} & \mathbf{0}_{3\times3} & \mathbf{T}_1 & \mathbf{0}_{3\times1} \\ \mathbf{0}_{3\times3} & \mathbf{0}_{3\times3} & \mathbf{0}_{3\times3} & \mathbf{0}_{3\times1} & \mathbf{0}_{3\times3} & \mathbf{T}_2 & \mathbf{0}_{3\times1} \\ \mathbf{0}_{3\times3} & \mathbf{0}_{3\times3} & \mathbf{0}_{3\times3} & \mathbf{0}_{3\times1} & \mathbf{0}_{3\times3} & \mathbf{0}_{3\times3} & -2\mathbf{T}_1\beta_2 \\ \mathbf{I}_3 & \mathbf{0}_{3\times3} & \mathbf{0}_{3\times3} & \mathbf{0}_{3\times1} & \mathbf{0}_{3\times3} & \mathbf{0}_{3\times3} & \mathbf{0}_{3\times1} \\ \mathbf{0}_{3\times3} & \mathbf{I}_3 & \mathbf{0}_{3\times3} & \mathbf{0}_{3\times1} & \mathbf{0}_{3\times3} & \mathbf{0}_{3\times3} & \mathbf{0}_{3\times1} \\ \mathbf{0}_{3\times3} & \mathbf{0}_{3\times3} & \mathbf{0}_{3\times3} & \mathbf{0}_{3\times1} & \mathbf{I}_3 & \mathbf{0}_{3\times3} & \mathbf{0}_{3\times1} \\ \mathbf{0}_{3\times3} & \mathbf{0}_{3\times3} & \mathbf{I}_3 & \mathbf{0}_{3\times1} & \mathbf{0}_{3\times3} & \mathbf{0}_{3\times3} & \mathbf{0}_{3\times1} \\ \mathbf{0}_{1\times3} & \mathbf{0}_{1\times3} & \mathbf{0}_{1\times3} & 1 & \mathbf{0}_{1\times3} & \mathbf{0}_{1\times3} & \mathbf{0}_{1\times1} \end{bmatrix}. \tag{89}$$

Finally, $-2\mathbf{T}_1\beta_2$ and $[\mathbf{T}_1^\top \quad \mathbf{T}_2^\top]^\top$ are of full column rank. So we have

$$\begin{bmatrix} \mathbf{0}_{3\times3} & \mathbf{0}_{3\times3} & \mathbf{0}_{3\times3} & \mathbf{0}_{3\times1} & \mathbf{0}_{3\times3} & \mathbf{I}_3 & \mathbf{0}_{3\times1} \\ \mathbf{0}_{1\times3} & \mathbf{0}_{1\times3} & \mathbf{0}_{1\times3} & \mathbf{0}_{1\times3} & \mathbf{0}_{1\times3} & \mathbf{0}_{1\times3} & 1 \\ \mathbf{I}_3 & \mathbf{0}_{3\times3} & \mathbf{0}_{3\times3} & \mathbf{0}_{3\times1} & \mathbf{0}_{3\times3} & \mathbf{0}_{3\times3} & \mathbf{0}_{3\times1} \\ \mathbf{0}_{3\times3} & \mathbf{I}_3 & \mathbf{0}_{3\times3} & \mathbf{0}_{3\times1} & \mathbf{0}_{3\times3} & \mathbf{0}_{3\times3} & \mathbf{0}_{3\times1} \\ \mathbf{0}_{3\times3} & \mathbf{0}_{3\times3} & \mathbf{0}_{3\times3} & \mathbf{0}_{3\times1} & \mathbf{I}_3 & \mathbf{0}_{3\times3} & \mathbf{0}_{3\times1} \\ \mathbf{0}_{3\times3} & \mathbf{0}_{3\times3} & \mathbf{I}_3 & \mathbf{0}_{3\times1} & \mathbf{0}_{3\times3} & \mathbf{0}_{3\times3} & \mathbf{0}_{3\times1} \\ \mathbf{0}_{1\times3} & \mathbf{0}_{1\times3} & \mathbf{0}_{1\times3} & 1 & \mathbf{0}_{1\times3} & \mathbf{0}_{1\times3} & \mathbf{0}_{1\times1} \end{bmatrix}, \tag{90}$$

which is of full column rank. Thus Ξ is of full column rank, and system (36) is observable.